



Evaluating Road-Cut Slope Stability Using Newly Proposed Stability Charts and Rock Microstructure: An Example from Dharasu-Uttarkashi Roadway, Lesser Himalayas, India

Anil Kumar Gupta¹ · Mrinal Kanti Mukherjee¹

Received: 23 June 2021 / Accepted: 3 March 2022 / Published online: 30 March 2022
© The Author(s), under exclusive licence to Springer-Verlag GmbH Austria, part of Springer Nature 2022

Abstract

The natural and cut slopes of a segment of the Dharasu-Uttarkashi Roadway (NH-108), located in the Lesser Himalayan Zone in India, have been studied for the first time adopting a multi-parametric integrated approach in terms of (1) distribution of magnitude of natural slope (2) engineering geological properties of intact rocks and rock masses, (3) kinematic analysis of slopes, (4) documentation of existing slope failures (5) rock- microstructural implications and (6) multiple geomechanical classification of slopes. Assessment of stability of slopes based on the combined study of the above parameters has been performed for twelve locations (L1–L12) on the road-cut sections where the slopes mostly have not yet failed. Magnitude of natural slopes overlooking the road section attains peak slope class of 41°–50°. Kinematic analysis characterizes the intact slopes in the above locations to possess conditions of wedge and toppling modes of failure, either in single or as combined. Existing failed slopes conform to combinations of planar, wedge, toppling and shallow circular failures. Rock microstructural study reveals development of strong shear-strength-weakening foliation anisotropy in the phyllites and schistose quartzites of the slopes that evidently serve as avenues of groundwater percolation and seepage and can promote failure along water-soaked foliation planes that ‘day-light’ on the road-cut slopes at locations L1, L8 L9 and L10. Based on Geomechanical classification systems applied to slopes including Continuous Slope Mass Rating, Q-Slope and Hazard Index, new stability charts have been developed that classify the slopes at each location to be one of the three types: severely unstable, unstable or stable. Based on the new stability charts, road-cut slopes at all twelve locations were found to be unstable and slopes at three locations – L7, L8 and L10 were observed to be severely unstable, particularly hazardous and require immediate mitigation.

Highlights

- Multiparametric integrated approach was adopted to study instability of road-cut slopes in the Dharasu-Uttarkashi highway for the first time New stability charts were developed combining three Geomechanical slope mass classification systems viz.
- the C-SMR, Q-Slope and Hazard Index.
- The impact of rock microstructure induced foliation anisotropy and water seepage along foliations and fractures on stability of slopes has been recognized.
- The stability of road-cut slopes were evaluated using newly developed stability charts and rock microstructure.

Keywords Stability chart · Stability assessment · Geomechanical classification · Kinematic analysis · Hazard index · Q-Slope

✉ Mrinal Kanti Mukherjee
mrinal_km67@yahoo.co.in

¹ Department of Applied Geology, Indian Institute of Technology (Indian School of Mines), Dhanbad 826004, India

1 Introduction

Slopes in road-cut sections in hilly terrains are prone to frequent slope failures at different scales that are due to combinations of variations of rock mass characteristics and factors

such as rainfall, blasting and traffic-induced vibrations and earthquakes. Furthermore, the stability of the rock slopes may also be influenced by road curvature especially in rugged terrains (Hoek and Bray 1981).

Several approaches for addressing slope stability problems are practiced. These include: (1) empirical approach, whereby a slope is assessed by rock mass classification systems and the quality of slopes is quantitatively classified, (2) Geometric and Kinematic approach which examines the potentiality of failure of a slope by analyzing the geometrical relationship of the orientations of discontinuity surfaces and the slope, (3) Limit equilibrium analysis that deals with the driving and resisting forces that act along an existing plane with the potential of failure and characterizes the stability of the slope in terms of safety factors, (4) Numerical analysis including Finite element analysis to deal with factor of safety of slopes in rock masses that do not contain any pre-existing planes or lines of failure. The empirical approach of assessing slope stability using rock mass classification system is often adopted as a first step for any transport engineering project. The advantage of applying Rock mass classification system in slopes is that, it can provide quantitative data and guidelines for engineering purposes and can improve originally abstract descriptions of rock mass from inherent and structural parameters (Liu and Chen 2007; Pantelidis 2009) by simple arithmetic algorithm (Romana 1985). Rock Mass classification system is therefore applied worldwide and facilitate characterization, classification and knowledge of rock mass properties. In empirical approach, slopes are geo-mechanically classified using rock mass classification systems.

Some of the existing geomechanical classification for slopes are: Rock Mass rating (RMR, Bieniawski 1989) Rock Mass Strength (RMS, Selby 1980), Slope Mass Rating (SMR, Romana 1985), Slope Rock Mass Rating (SRMR, Robertson 1988), Mining Rock Mass Rating (MRMR, Laubscher 1990), Mining Rock Mass Rating modified (MRMR modified, Haines and Terbrugge 1991), Chinese Slope Mass Rating (CSMR, Chen 1995), Natural Slope Methodology (NSM, Shuk 1994), Modified Rock Mass Rating (M-RMR, Unal 1996), Geological Strength Index (GSI, Marinos and Hoek 2000, 2001), Modified GSI (Sonmez and Ulusay 1999, 2002), Slope Stability Probability Classification (SSPC, Hack 1998, Hack et al. 2003), Modified Slope Stability Probability Classification (SSPC modified, Lindsay et al. 2001), Continuous Rock Mass Rating (CRM, Sen and Sadagah 2003), Continuous Slope Mass rating (Continuous SMR, Tomás et al. 2007, Tomás et al. 2012), Alternative Rock Mass Classification System proposed by Pantelidis, 2010, Slope Stability Rating (SSR, Taheri and Tani 2010), Q-Slope classification (Barton and Bar 2015; Bar and Barton 2017) and Modified Rock Mass Rating by modified

blockiness index (RMR_{mbi} , Chen and Yin 2020). Slope stability assessment in road-cut sections is widely practiced using several of the above methods (cf. Kentli and Topal 2004; Umrao et al. 2011; Gupta and Tandon 2015; Basahel and Mitri 2017; Pradhan and Siddique 2020). However, it has been commonly observed that each scheme of geomechanical classification of slopes as stated above, may indicate varying stability grades of slopes that differs from one another. In other words, a slope that is classified as unstable in one classification scheme may get classified as stable in another. Therefore, development of stability charts combining more than one classification schemes seems acutely necessary for a comprehensive judgment of slope stability of a particular locality.

In this paper, we present the results of a comprehensive study of slopes by integrating multiple parameters including natural slope distribution, causes of existing failed slopes, geometric and kinematic analysis of cut slopes, analysis of new field data on structural elements and cut slopes, laboratory testing of representative rock specimens that occur on slopes, geomechanical classification of slopes and rock-microstructural implications on slope failure to assess the stability of intact slopes in a part of Dharasu-Uttarkashi road section (NH 108), in Uttarkhand in India. *A novel set of stability charts is developed that combines more than one geomechanical classification of slopes.* The studied segment of the roadway is located in a landslide prone area in the lesser Himalayas where several shallow landslides occur. The roadway connects Tehri and Uttarkashi and is an important transport way that supports business, pilgrimage, infrastructure development and international tourism round the year. In the event of no systematic study hitherto existing on stability analysis of road-cut slopes in the studied section, the present study accounts for comprehensive stability assessment of cut slopes for the first time, based on the proposed novel stability charts and rock microstructure.

2 Geologic Setting, Seismicity and Climate of the Study Area

2.1 The Study Area

The study area falls within the Survey of India Toposheet number 53 J/6 and is confined between Dharasu bend and Dunda (Fig. 1). The Dharasu-Uttarkashi roadway is the national highway no NH 108 and is the route to go to Gangotri. At Dharasu, the road bifurcates at a sharp bend (Dharasu bend) (Fig. 1) with one part connecting Dharasu and Uttarkashi and onwards to Gangotri whereas the other part links Dharasu and Yamunotri. The Bhagirathi River moves parallel to the Dharasu-Uttarkashi Road segment.

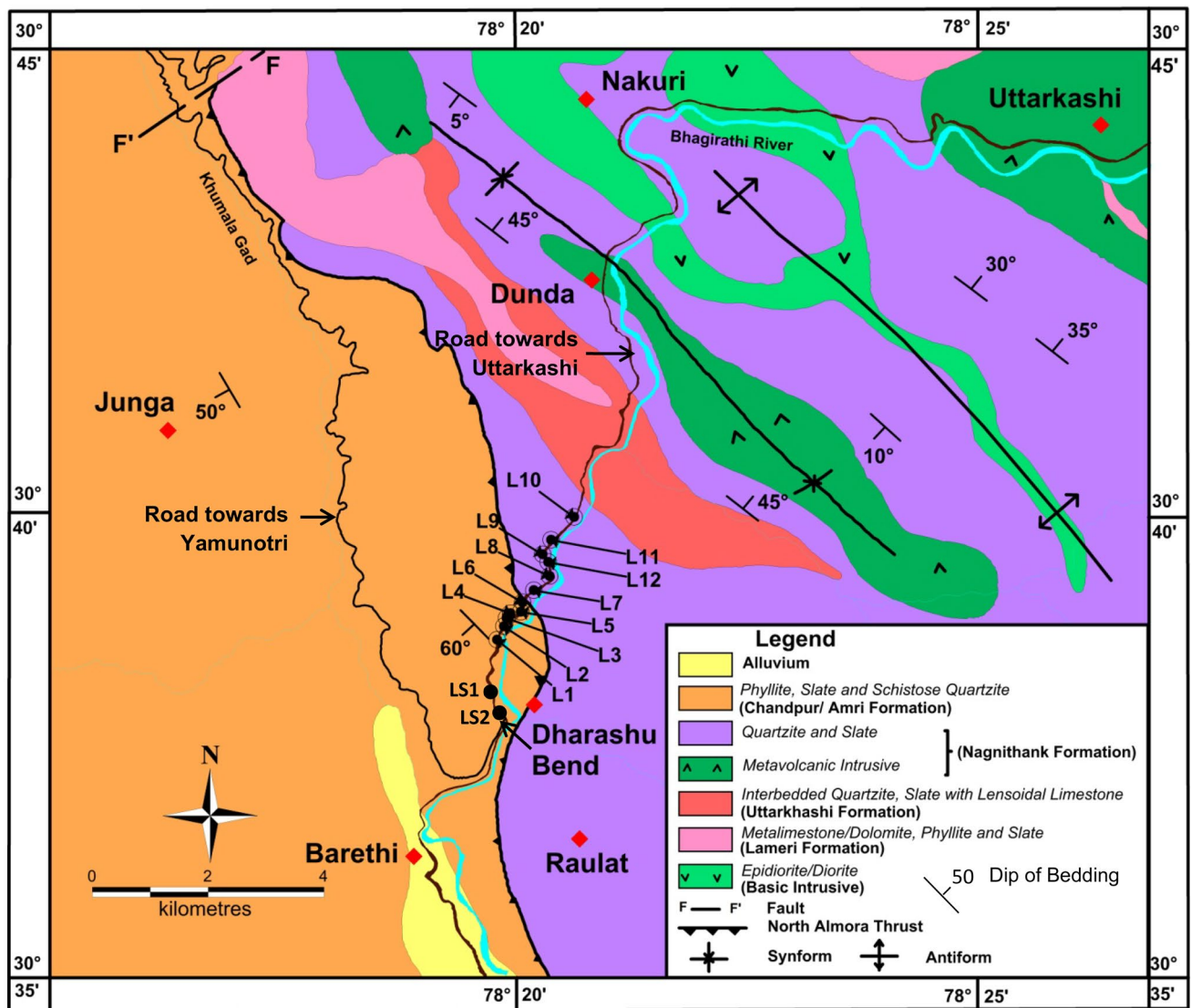


Fig. 1 Geological Map of the study area. Studied slope locations are marked as L1, L2... etc. on the Dharasu-Uttarkashi Road section (NH 108). The Dharasu bend (indicated by arrow) is a junction between the two road sections: one leading to Yamunotri Glacier through

Khumla Gad in the north-west and the other one leading to Uttarkashi in the northeast. Shallow landslides occur at locations LS1 and LS2 on the road near Dharasu bend

2.2 Site Geology

The study area forms a part of Lesser Himalayan Sequence of rocks of the Garhwal Himalayas of northern India. The lesser Himalayan sequence corresponds to 1870–800 Ma age and is comprised of meta-sedimentary and meta-volcanic strata and Augen gneiss (Yin 2006; Jain et al. 2016). The Lesser Himalayan rocks that are exposed in this region belong to the Neoproterozoic Jaunsar Group and the Mesoproterozoic Garhwal Group with the North Almora thrust (NAT) separating the two Groups (Fig. 1). Two formations that are equivalent to each other constitute the Jaunsar Group Shanker et al. 1989, Sharma and Singh 2005. These are the

Chandpur/Amri Formation that are exposed near Dharasu bend and the equivalent Morar–Chakrata Formation that outcrops around Junga (Fig. 1). The Jaunsar Group occurs on the west to south-western side of the NAT and forms a part of its hanging wall. The formations are lithologically composed of phyllites, slate, graywacke, schistose quartzites and basic intrusives.

The relatively older Garhwal Group is exposed in the eastern to north-eastern side of the NAT (Fig. 1). Three Formations constitute the Garhwal Group in the region that outcrops between Uttarkashi and the NAT. These are, from relatively older to younger: Uttarkashi, Lameri and Nag-nithank Formation. The Uttarkashi formation consists of

Table 1 Stratigraphy of the Lesser Himalayas in the study area

Age	Group	Formation	Lithology
Pleistocene to Holocene	Quaternary Deposits	–	Unconsolidated to semi consolidated assemblage of Clay, Sand, gravel boulder and pebbles in various proportions
Neoproterozoic	Jaunsar Group	Chandpur Formation (= Morar-Chakrata Formation)	Phyllite, Slate meta-graywacke, quartzites and basic intrusive
-----North Almora Thrust (South-westerly dipping out- of -sequence thrust)-----			
Mesoproterozoic	Garhwal Group	Nagnithank Formation Lameri Formation Uttarkashi Formation	Quartzites and slates with metavolcanics Limestone, dolomite, phyllite and slate Interbedded quartzite, slate, with lensoidal limestone; gray, green and purple slates with quartzite
-----Main Central Thrust (North-easterly dipping thrust)-----			
Undifferentiated proterozoic	Central Crystalline Group	Wazri Formation Yamunotri Formation	Chlorite-Biotite-Garnet-Graphite schist, porphyroblastic garnet gneiss, tourmaline garnet gneiss, marble, quartzite and basic intrusives Sillimanite-Kyanite bearing schist and gneiss, garnetiferous biotite schist, migmatite and basic intrusives

interbedded quartzite and slate with lensoidal limestone. The Lameri consists of interbedded limestone, dolomite, phyllite and slate and the Nagnithank is composed of interbedded quartzites, slates and metabasalts.

To the northeast of Uttarkashi, the Garhwal Group is limited by the Main Central Thrust (MCT)-an important tectonic salient. The MCT dips toward northeast and its hanging wall exposes the Central crystalline Group consisting of the Wazri and the Yamunotri Formations. The stratigraphic framework of the study area is presented in Table. 1.

The Dharasu-Uttarkashi roadway cuts through the Jaunsar, NAT and the Garhwal Group of rocks as described above and expose the rocks on the cut-slope face. The hanging wall of the NAT is in the form of an antiform that plunges due SSE. The NAT conforms with an out-of-sequence thrust (antithetic thrust) that dips towards west to southwest (Fig. 1). The Garhwal Group of rocks in the foot-wall side (eastern side) of the NAT is folded into a NW – SE trending antiform-synform pair. The synform occurs near Dunda (Fig. 1) and the corresponding antiform occurs near Nakuri (Fig. 1).

2.3 Seismicity and Climate

The study area lies within Zone-IV of the Seismic map of India and is therefore not a safe place for human settlement. The Uttarkashi earthquake of October 20, 1991 (M_s 7.0 USGS) and the Chamoli earthquake of March 29, 1999 (M_s 6.6 USGS) were devastating seismic activity recorded in

the region. The entire area between Main Boundary Thrust (MBT) and MCT i.e., the entire Lesser Himalaya is beset with high peak ground acceleration values between 0.3 g and 0.5 g over a short distance spanning 25 km to 40 km (Kumar et al. 2011). This is indicative of a high seismic hazard zone in the study area and beyond.

The climate is in general warm and temperate. The Köppen-Geiger classification of climate in the area is Cwa. The summers are marked by relatively more rainfall than the winters. The temperatures vary between minimum 3 °C (in January) and maximum 33 °C (in June) with an average temperature of 18 °C. The lesser Himalayas acts as an orographic barrier to the moisture-laden winds from the south and induces a medium rainfall pattern in the study area. Analysis of historic precipitation data, obtained from Kharsali Rain gauge station in Uttarkashi and World Weather online website:

(<https://www.worldweatheronline.com/lang/en-in/dharasu-weather-history/uttarakhand/in.aspx>) reveal a mean multi-annual (from 2009 to 2019) rainfall of 761.31 mm (Fig. 2a). The monsoon spans from June to September and the cumulative rainfall during monsoon may exceed 1000 mm (Fig. 2b). It can be observed from Fig. 2b, that August remained the rainiest month from 2009–2012 and was replaced by July during 2013–2018. Relative contribution of mean rainfall of each monsoon month to the cumulative mean annual rainfall (Fig. 2c) shows that precipitation in the month of August, in general, contributes maximum to the cumulative rainfall during the monsoons.

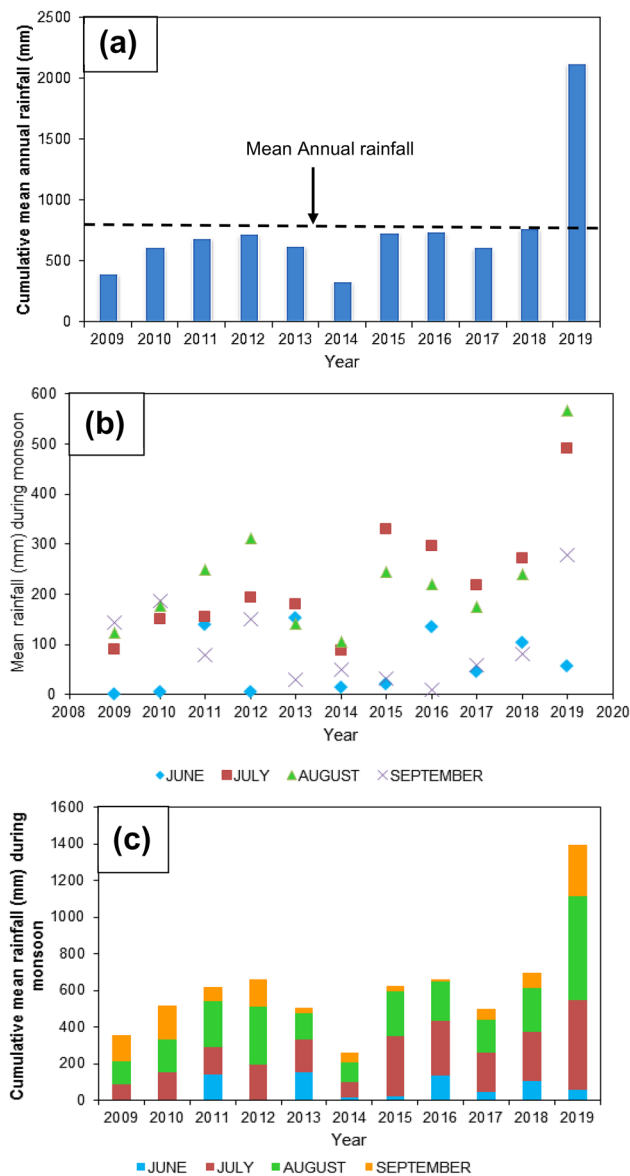


Fig. 2 Rainfall data of the study area. **a** Cumulative multi-annual mean precipitation over the past decade. **b** Distribution of mean annual precipitation during the monsoon months from June to September over the past decade. Note that August remained the rainiest month from 2009 to 2012 and was replaced by July during 2013–2018. **c** Relative contribution of mean rainfall of each monsoon month to the cumulative mean annual rainfall

3 Methodology

The methodology used in this study is illustrated in the form of a flow-chart diagram in Fig. 3. It begins with evaluating natural topographic slopes related to the road-cut section of the study area based on satellite imageries and topographic maps. Based on this evaluation, zones on highway sections were identified where slopes are anticipated to fail. The second step involves an intensive field

investigation based on the above study and includes observations, measurement and documentation of already failed slopes if any, lithology, penetrative and non-penetrative structures, slope characteristics and oriented rock sample collection by continuous walk-over method. The third step involves determination of physical and engineering properties of rock samples collected from the field locations, by laboratory testing. The fourth step is to perform the kinematic analysis of slopes at each location. The kinematic analysis has been performed from the orientation data of joint sets and slope to examine the possibility of failure and its type. The fifth step is to perform a detailed rock-microstructural study to evaluate the role of mineral grain boundary anisotropy and preferred dimensional orientation of constituent minerals in failure of slopes. In the sixth step, the Rock Mass rating RMR for each location was determined by the Discrete Rock Mass Rating System (Bieniawski 1989). The seventh step in the methodology is to perform a slope mass rating using the results of the kinematic analysis, the joint-slope orientation relationships, and the RMR score. Five systems of geomechanical classification of slopes viz. original SMR (Romana 1985), Chinese SMR (Chen 1995), Continuous SMR (Tomás et al. 2007), Q-slope (Bar and Barton 2017) and Hazard Index (HI) (Pantelidis, 2010) were applied to structurally controlled failure of road-cut rock slopes. For non-structurally controlled failure of road-cut rock slopes only the HI method is used. A novel scheme of stability field chart is developed by combining the various systems of geomechanical classification of slopes. Finally integrating results and information from all the above parameters, the stability of the slopes of the road-cut section of the study area has been comprehensively assessed within the framework of proposed stability charts and microstructural implications.

4 Studied Parameters and Their Results

4.1 Natural Topographic Slope Distribution

The study area is marked by a rugged topography and is a part of north to south flowing Bhagirathi River watershed. The maximum and minimum elevation points of the watershed are 2300 m and 869 m respectively with a relief difference (Rd) of 1431 m. The drainage is dendritic to parallel with a drainage density (Dd) of 3.02 km/km². The ruggedness number (Rn) expressed as $Rn = [(Dd \times Rd)/1000]$ is determined to be 4.32 and is considered to be relatively high due to deep dissection by the Bhagirathi River and its tributary valleys. Ruggedness number combines the slope steepness and length indicating the extent of the

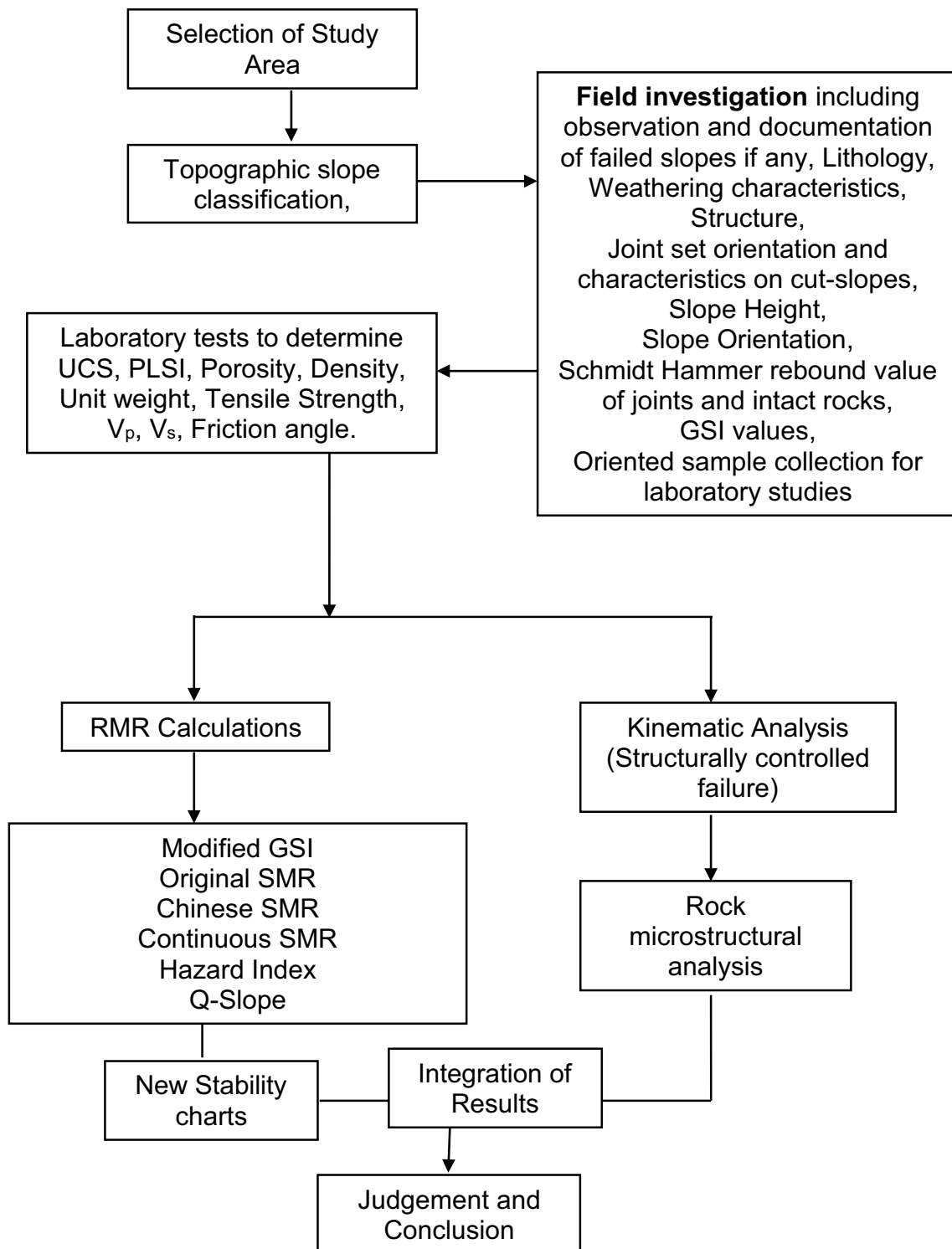


Fig. 3 Flow chart of the methodology adopted in this work

instability of land surface (Strahler 1957). High ruggedness number would therefore signify steep slopes. The Dharasu-Uttarkashi Road section in the study area therefore has

steep natural slopes overlooking the road. For estimating the natural topographic slope distribution in the study area 1:50,000 topographic map of Survey of India, has been

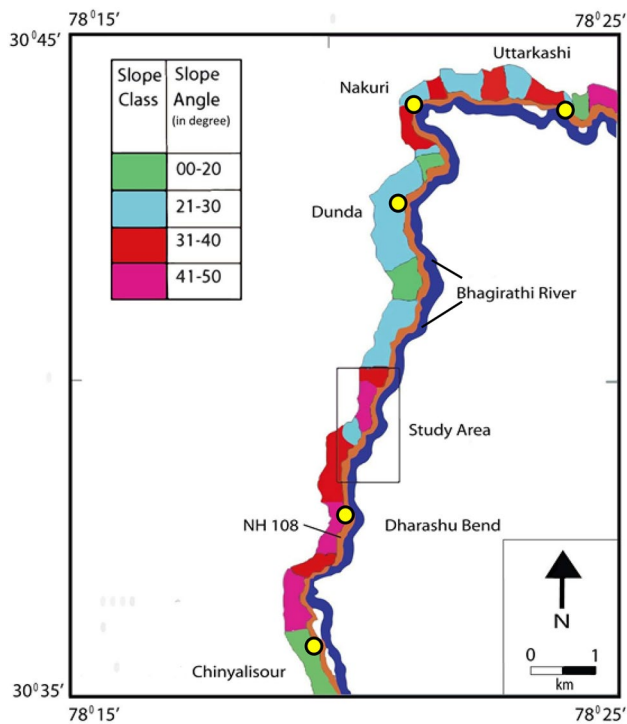


Fig. 4 Natural Slope map of the Dharasu-Uttarkashi Road section (NH-108). The study area is shown with a rectangular outline. The slopes overlooking the road are documented in four classes with the gentlest slope class 0° – 20° and a steepest slope class of 41° – 50° . The Bhagirathi River runs approximately parallel to the road section

used. Individual segments were defined by the spur that is flanked by adjacent valleys. Topographic slope angle was determined for each spur from the trigonometric ratio of the shortest map distance from the highest elevation of the spur to the road level and the total elevation obtained from the number of elevation contours in between the road and the highest point of the spur. Frequencies of slopes in degrees of consecutively adjacent segments were recorded and grouped into slope classes and are documented in Fig. 4. The results show that the natural slopes overlooking the roadway in the study area can attain a slope of 41° – 50° at several segments (Fig. 4). These natural topographic slope segments were further studied in Google Earth Engine by zooming to a scale of 1:1000 and slopes were determined trigonometrically from the ratio of distance from the road level to the nearest slope break along the topographic slope and its corresponding elevation. No attempt was made to remove vegetation cover from Google Earth images during slope determination. This scale of resolution provides the site-specific slope that ranges 55° – 70° . Such high natural topographic slope segments may pose instability along road cuts at several locations and were planned for direct field investigation and slope stability assessment.

4.2 Slope Failure Incidences

The study area reveals that even though the study area is rugged with steep natural slopes and the area is seismically active with an average annual rainfall of ~ 760 mm for the last decade, no slope failures occurred in the study area before the year 2011 (Fig. 5a). In 2011, there were several cut sections of the road that failed (shown by arrows in Fig. 5b). New failure zones were subsequently added along with erosion-induced modification of earlier-failed slopes in subsequent years (Fig. 5c, d). The shallow landslides near Dharasu bend (LS1 and LS2 in Fig. 1) occurred during peak precipitation during August 2011 in presence of an ongoing road widening construction work that adopted uncontrolled blasting. Vibrations from uncontrolled and unsystematic blasting at the road and cut-slope intersection, coupled with heavy spells of rainfall during monsoon months, is attributed to the cause of the failure. The debris from the slope failure events were periodically removed to make the highway functional despite getting blocked by new failure events (Fig. 6a).

Failed slopes conform to either single or a combination of several types of failures including rock fall, plane failure, wedge failure, toppling and circular failure (Wyllie and Mah 2004). For example, a combination of rock fall and wedge failure has occurred at location no. L10 (Fig. 6a). Incipient failure zones with spalling of steep cut slopes can be ascertained from observations like rotation of trees and other vertical markers (Fig. 6b). Shallow circular slope failures are observed near Dharasu bend (Fig. 6c, 6d) with their corresponding locations LS1 and LS2 indicated in Fig. 1.

In addition to the above, there are several locations where the road-cut slopes apparently have a possibility of failure. For instance, plane failure is anticipated in Fig. 7a, wedge failure in Fig. 7b, c, combination of planar and wedge sliding in Fig. 7b, and toppling failure in Fig. 7d.

4.3 Field Data and Observations

Outcrops of every location and in between was examined in the field by walk-over method. Important observations that were relevant to the stability assessment of slopes were performed along with measurement and documentation. These include, rock type, variation in rock composition and grain size if any, structures including compositional banding, folds, joints, faults, penetrative foliations, lineations, weathering characteristics, geological strength index (GSI), Schmidt hammer rebound value of joints and intact rocks, joint characteristics including joint frequency, joint persistence, joint aperture and filling, joint surface roughness, orientation of structural elements, orientation of slope, magnitude of slope – height, curvature & areal extent, road

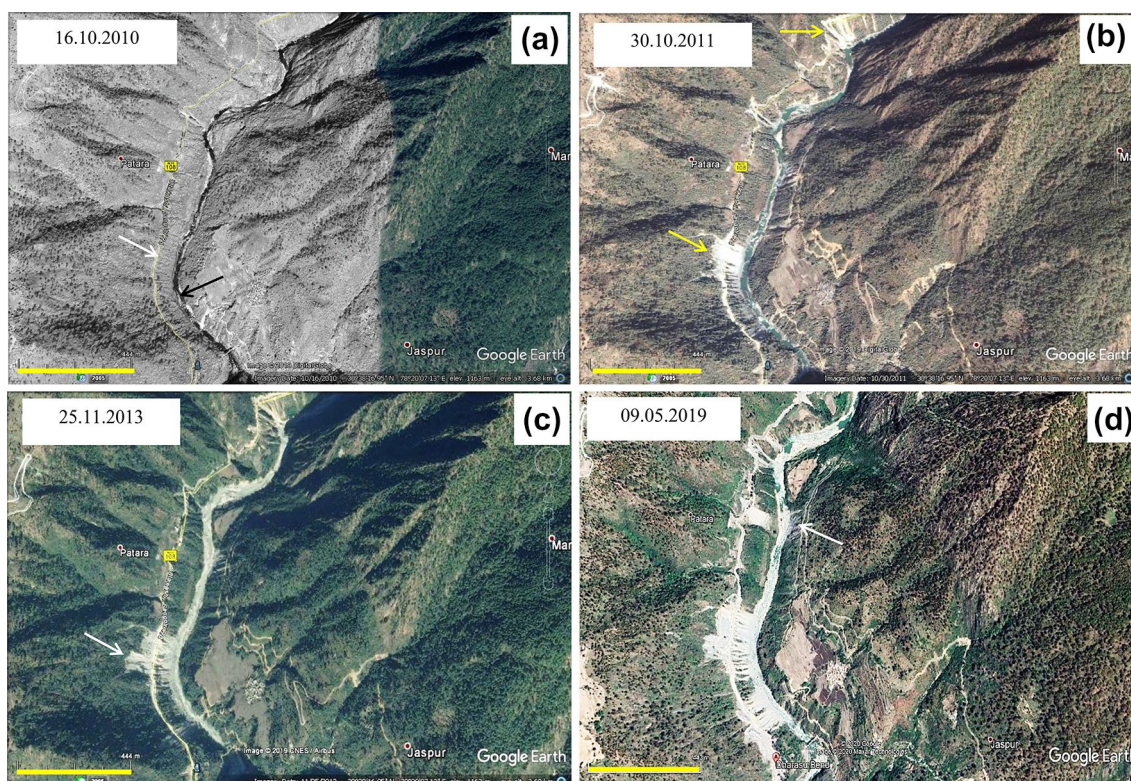


Fig. 5 Google Earth images of the study area before and after slope failures. Insets contain the date of the image. **a** Image before slope failure. The Dharasu-Uttarkashi Road section (white arrow) runs parallel to the Bhagirathi River (black arrow). **b** Slope failures along

the road-cut section occur at several places. The prominent ones are indicated by arrow. **c** Slope failures in new areas (marked by arrow) located south of the earlier-failed zones. **d** Slope failures on the eastern bank of Bhagirathi River (marked by arrow). Scale bar is 444 m

orientation and groundwater conditions. Oriented samples were collected from the locations for laboratory study. Twelve locations (L1–L12) were identified during fieldwork, where the slopes were anticipated to fail. Table 2 gives the summary of measured data of the locations L1 to L12 in the field. The slope heights of the cut slopes vary in the range of 8–30 m. Cut Slopes are steep to very steep and range 55° – 80° . Location L1 possesses five joint sets; L2, L4, L5, L7, L8 and L10 possesses four sets of joints whereas L3, L6, L9, L11 and L12 possesses three joint sets. Penetrative foliations (schistosity in schistose quartzites and slaty cleavage in phyllites and slates) have a mean orientation of 62° – 28° with dip angles of foliation in the range of 45° – 70° and azimuth in the range of 25° – 37° . Data presented in Table 2, in addition to the above, were used to derive other parameters that are subsequently discussed below.

4.4 Engineering Geological Properties of Rock Samples

The engineering geological properties of all the rock types exposed in the study area have been evaluated on the basis of field observations and laboratory tests including, density,

effective porosity, unit weight, point load strength index (PLSI), Uniaxial compressive strength (UCS), Schmidt hammer rebound value (R value), tensile strength (Brazilian test), and ultrasonic wave velocities (both P- and S-waves). The tests were carried out according to ISRM (1981) and the laboratory setting, sample installation and test results for PLSI, Brazilian test and UCS are illustrated in Fig. 8. Table 3 presents the data of the laboratory tests performed in the cored specimens of oriented representative samples of the slope locations. Each test has been repeated five times for each parameter for each type of rock and the mean value has been presented in the Table 3.

4.5 Kinematic Analysis of Slopes

Assessment of slope stability begins with a geometric and kinematic analysis of slopes that involves analysis of the orientation relationships between the discontinuities and the slope in question. Kinematics refers to the motion of bodies without reference to the forces that cause them to move. In general, geometric relationships between discontinuities and slope indicate the possibility of movement of blocks of rocks bounded by discontinuities. If the kinematic analysis

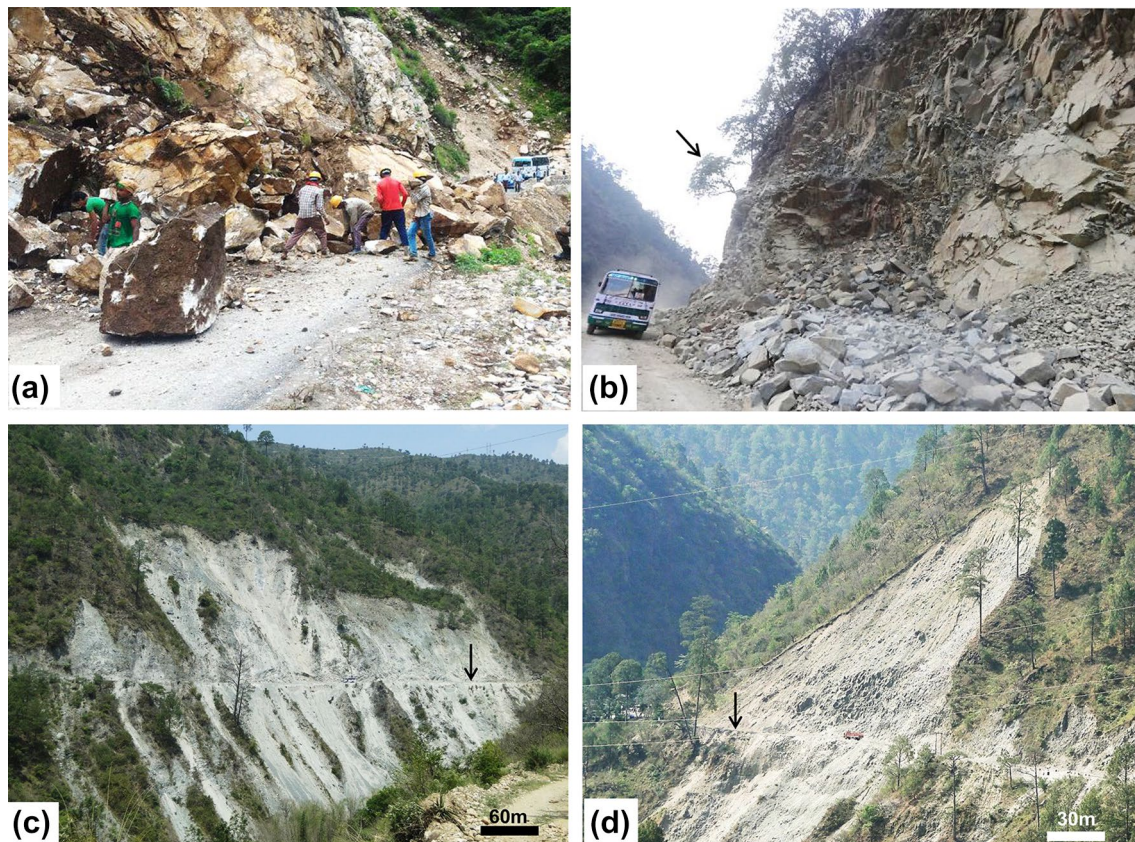


Fig. 6 Failed slopes in the Dharasu–Uttarkashi Road section in the study area. For locations refer to Fig. 1. **a** Wedge blocks and boulders produced by wedge failure at location L8. Traffic has been halted for clean-up operations. **b** Spalling of rock and wedge failure at location L10. Ongoing creep movements on slope are evident from rotation

of tree (indicated by arrow) on the cut slope. **c** Shallow landslides composed of mixed soil and rock fragments at location 800 m north of Dharasu bend (LS1 in Fig. 1). Arrow indicates the road level. **d** Shallow landslides occurring at 150 m north of Dharasu bend (LS2 in Fig. 1) Arrow indicates road level

indicates that the failure controlled by discontinuities is likely then the stability further needs to be evaluated by a limit equilibrium analysis which considers the shear strength along the failure surface, the effects of pore water pressure and the influence of external forces such as reinforcing elements and earthquakes (Turner and Schuster 1996).

Kinematic analysis leads to recognition of three types of failure: plane, wedge and topple, using conditions and criteria for each type of failure (Hoek and Bray 1981; Goodman 1989; Wyllie and Mah 2004). A plane failure develops when the dip amount of a discontinuity plane is less than the dip amount of the slope measured in the direction of sliding and is greater than the friction angle of the discontinuity, provided that the strikes of the discontinuity and the slope are parallel or nearly parallel within certain limits ($\pm 20^\circ$). A wedge failure is recognized when the plunge amount of the line of intersection of two discontinuities is less than the dip amount of the cut slope and exceeds the friction angle, provided that the plunge direction of the intersection line is same as that of the dip direction of the slope within certain limits ($\pm 40^\circ$). A toppling failure is indicated when the

dips of the slope and the discontinuity planes are oppositely directed within certain limits ($\pm 10^\circ$) and the dip amount of the discontinuity and the slope exceeds 60° .

In this study, the kinematic analysis is done for all of the cut slopes of the highway in the study area, distributed over twelve locations (numbered L1 to L12 serially). For the kinematic analysis the lower hemisphere stereographical projection method is used as described by Hoek and Bray (1981) and Goodman (1989). From field observations it is evident that the strike of the cut slopes at each location is parallel to the trend of the highway and is therefore accordingly considered. Kinematic analysis was performed using DIPS 6.0 of Rocscience Inc. 2014 and the failure modes were identified for each location as illustrated in Fig. 9. The summary of the kinematic analysis for each cut slope is presented in Table 4. From the kinematic analysis it can be inferred that slopes at locations L6, L10, L11 and L12 tend to have wedge failure instability, slope at location L9 possesses toppling failure instability whereas slopes at – locations L4 have both plane and wedge failure instability, L7 has both plane and toppling failure instability and L1, L3 and L8 possess both

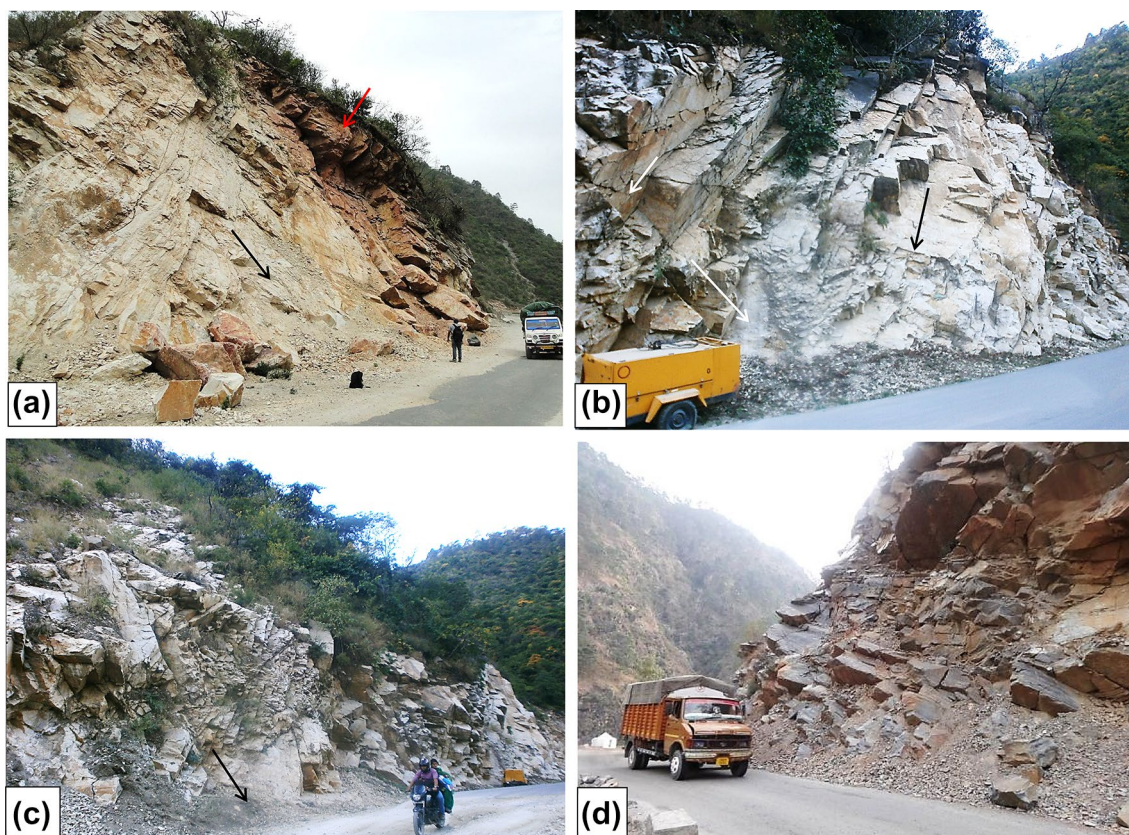


Fig. 7 Failure types of slopes anticipated to fail. For locations refer to Fig. 1. **a** Plane (black arrow) and toppling (red arrow) failure expected at poorly excavated slope at location L7. Plane failure has already occurred and the failure planes are exposed; **b** Plane (black arrow) and wedge (white arrow) failure expected at location L4 with arrow indicating the down-sliding sense. **c** Wedge failure conditions

with arrow indicating the direction of probable movement of wedge at location L11. **d** Dominantly Toppling failure condition at location L9. Although minor planar failure surfaces dips towards road due to random joints, in general planar failure is not the mode of instability in the area

wedge and toppling failure instability. Based on kinematic analysis, locations L2 and L5 do not show any indications of structurally controlled failure.

4.6 Rock Microstructure

Microstructural study was performed in the oriented thin sections of the rocks of all the locations of the study area from representative samples to understand the control on stability of slopes by anisotropy & inhomogeneity of the rocks that arise out of the variation in mineralogical composition, grain size, grain orientation, grain boundary geometry, texture and microstructure of the rocks. Thin sections were prepared by cutting the oriented specimen orthogonal to foliation and parallel to the elongated mineral lineation observed on the foliation plane. In this section, an account of composition and microstructure of rocks from the slopes of the study area is presented and the effect of rock microstructure on stability of slopes will be explained at a later stage (see Sect. 5.5).

The white and gray quartzite are hard rocks and in general, are composed of dominantly quartz (~85–90% by volume) and minor mica (~10–15% by volume) (Fig. 10a). The quartz grains in quartzite manifest a bimodal grain size consisting of a relatively coarse size population that range 100–250 μm and a relatively fine-grained population ranging 10–40 μm . The coarse grains correspond to the framework detrital clasts whereas the relatively fine-grained population corresponds to dynamically recrystallized quartz grains. The ratio of volumetric proportion in which the detrital quartz and recrystallized quartz populations occur in quartzite is ~9:1. Detrital quartz grains in quartzite, manifest two distinct types of grain boundary contact geometry. The first type (Type-I contact) is of straight to moderately curved (embayed) sharp contact between the grains that, in most instances, are parallel to the long dimension of the grains in contact (Fig. 10a). They define a preferred alignment of the quartz grains and thereby define the rock cleavage (S1). The cleavage planes are therefore defined by the continuity of the grain

Table 2 Summary of field data of different location and failure types

Location	Rock type	GSI	Slope Height (m)	Slope face (dip/dip direction) (Degrees)	Foliation (dip/dip direction) (Degrees)	Orientation of joints (dip/dip direction) (degrees)						Potential Failure types (from kinematic analysis)		RMR
						J1	J2	J3	J4	J5	Plane (P)	Wedge (W)	Topple (T)	
L1	Schistose Quartzites with interbands of phyllite	45–50	8	75/80	65/32	66/195	26/360	40/145	31/240	80/110	×	✓	✓	64
L2	Quartzites with interbands of phyllite	48–55	10	65/125	70/30	60/230	30/60	80/120	27/135	a	×	×	×	68
L3	Light Gray Quartzites	50–55	11	60/120	60/28	51/330	55/195	55/120	a	a	×	✓	×	73
L4	Light Gray Quartzite	55–60	23	80/90	65/37	47/118	50/03	60/230	19/60	a	✓	✓	×	73
L5	White Quartzite	55–60	17	80/90	a	53/150	50/15	55/240	23/55	a	×	×	×	73
L6	Quartzites with interbands of phyllite	55–60	20	70/140	45/28	50/240	43/03	45/200	a	a	×	✓	×	75
L7	White Quartzite and metavolcanics	60–65	27	75/160	55/30	56/240	38/30	60/330	43/160	a	✓	×	✓	73
L8	Quartzite with slate interbeds	50–55	30	80/60	65/25	51/230	16/350	63/20	75/350	a	×	✓	✓	75
L9	Dark Gray Quartzite with interbeds of slate	55–60	15	60/90	60/35	60/250	35/0	51/130	a	a	×	×	✓	73
L10	Phyllite with interbeds of Quartzite	35–40	26	75/90	70/30	55/210	30/50	70/350	75/150	a	×	✓	×	49
L11	Schistose Quartzite	45–50	10	55/160	68/28	43/230	55/30	70/180	a	a	×	✓	×	64
L12	Dark Gray Quartzite	50–55	18	70/130	a	65/10	52/160	70/270	a	a	×	✓	×	66

a absent, ✓ kinematically possible, × kinematically not possible



Fig. 8 Laboratory experimental set up for determining engineering geological properties of intact rocks. **a–c** Point load Strength Index (PLSI); **a** equipment set up, **b** specimen under test, **c** Specimens after first round of PLSI test; **d–f** Brazilian test; **d** equipment set up, **e** specimen for test loaded between platens before testing, **f** specimen after test; **g–i** uniaxial compressive strength (UCS); **a** The Univer-

sal testing machine equipment set up with pressure control and dial gauge on the right and the 1000 Kilo Newton compressing unit on the left, **b** Specimen for test with attached strain gauges for determining strain at peak failure load during UCS determination, **i** specimen after test

contacts (Fig. 10a). The second type of grain contacts (Type-II) are at high angles to the cleavage plane contacts and are strongly embayed within one another and frequently show serrated outline (Fig. 10a). Type-I contacts reflect truncation of an otherwise smooth boundary of a rounded quartz against another grain at the contact and would imply a pressure-solution mechanism origin of

the truncated grain contact whereby both grains undergo dissolution at the contact under the existing compressive stress directed orthogonal to the cleavage during tectonic deformation. Occasionally Type-II contacts are characterized by a zone of mica fibers that grow orthogonal to the grain boundary and parallel to the cleavage (Fig. 10a) thus defining a pressure shadow. Some of the Type-I contacts

Table 3 Engineering geological properties of representative rock specimens of the study area determined by laboratory tests

Rock type	Outcrop locations in the study area	Porosity(η) (%)	Density (gm/cm ³)	Unit Weight (γ) (kN/m ³)	Schmidt Hammer reboundvalue(R)	UCS (MPa)	PLSI(ISO50) (MPa)	Brazilian/Tensile Strength (MPa)	V_p (km/s)	V_s (km/s)
White quartzite	L1, L2, L5, L6, L7, L8	0.565	2.639	25.83	64	227.89	10.36	13.12	5.56	1.30
Light gray quartzite	L3, L4	0.614	2.649	25.78	66	285.64	12.98	16.81	4.92	1.20
Dark gray quartzite	L9, L12	0.719	2.710	26.67	62	106.35	4.84	13.29	4.66	2.04
Metavolcanic Rock	L7	0.422	2.99	29.32	70	396.47	18.02	20.76	6.0	2.36
Phyllite	L10, L11	2.021	2.727	26.75	35	30.27	1.38	1.72	2.27	0.88

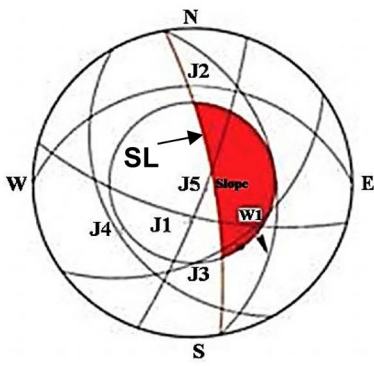
are occasionally serrated (Fig. 10a) and sometimes contain mica films (Fig. 10a). Serrated outline in both Type-I and Type-II contacts are attributed to grain boundary migration recrystallization with the development of subgrains at the contact (Urai et al. 1986; Passchier and Trouw 2005). In contrast to recrystallized quartz grains, detrital quartz grains show undulose to patchy extinction patterns that attest to intra-crystalline deformation of quartz (Fig. 10a).

The volumetric proportion of mica in schistose quartzite varies in the range of 15–30%. When volumetric proportion of mica is relatively higher (~30% by volume), the cleavage is continuous and is defined by the strong dimensional preferred orientation of both mica and quartz grains (Fig. 10b) with the mica-rich cleavage seams being relatively more continuous, thick and anastomosing around the detrital quartz grains. Mica are often bent in the anastomosing cleavage seams (Fig. 10b) and volume proportion of recrystallized quartz grains increase to give a detrital grain–recrystallized grain ratio of ~4:1.

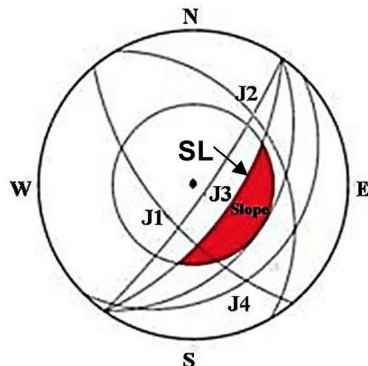
In schistose quartzites, fibers of quartz-mica aggregates give rise to “quartz-mica beard” microstructures on the Type-II grain boundaries of detrital quartz grains that are nearly orthogonal to cleavage (Fig. 10b) with the long dimension of the fibers parallel to the cleavage. Quartz grains belonging to the larger size fractions, show frequent fracturing (Fig. 10a) in addition to their intra-crystalline deformation with sometimes conjugate fractures in a single grain. However, frequency of fracturing apparently decreases with increase in the volume percentage of mica (Fig. 10b).

Phyllites are mineralogically composed of 60–80% mica and 20–40% quartz with a size range of 2–30 μm for mica and 2–50 μm for quartz. In phyllites, the cleavage conforms to domainal schistosity as described by Powell (1979), with zones of mica aggregates having strong preferred orientation, defining the cleavage domains (Fig. 10c) and an assemblage of quartz grains constituting the microlithon domains (Powell, 1979; Gray, 1978) that alternate with cleavage domains (Fig. 10c). In general, in the microlithons, the quartz grain aggregates show a weak preferred orientation parallel to the cleavage but the relatively less proportion of mica grains show a strong preferred orientation parallel to the cleavage (Fig. 10c). Even though mica grains are, in general, straight and parallel to the cleavage, several of them are kinked (Fig. 10c) in both domains.

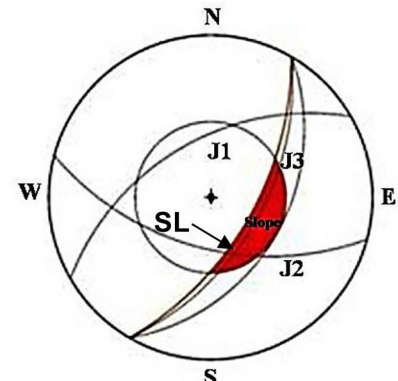
In Schistose quartzites and phyllites, there are microscale evidences of water percolation along foliation planes; for example, in Fig. 10d the locus of the water percolation is marked by ferruginous stains that result due to precipitation of dissolved iron from the percolating water. The stains are multiple and are anastomosing but follow the cleavage in general. This indicate that water percolation affects the rock as a whole over large areas and are networked to produce zones of seepage along foliation planes.



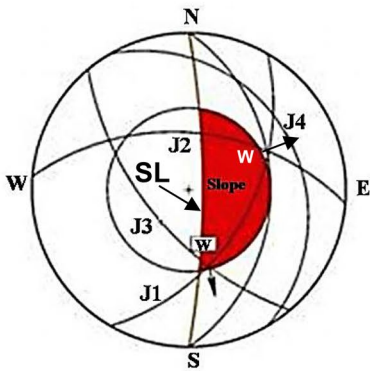
L1: Wedge Failure, Toppling



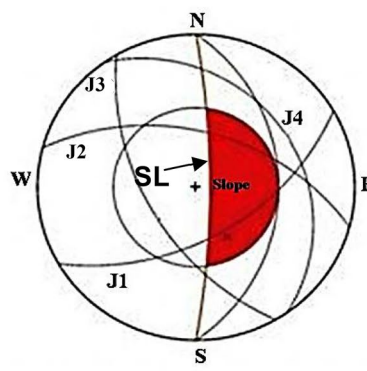
L2: No Failure



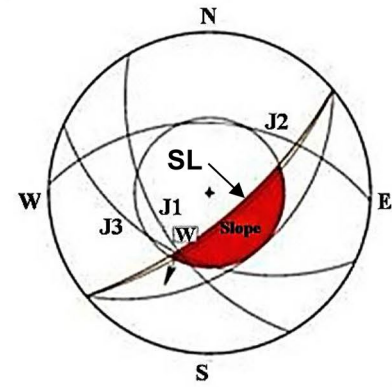
L3: Wedge Failure, Toppling



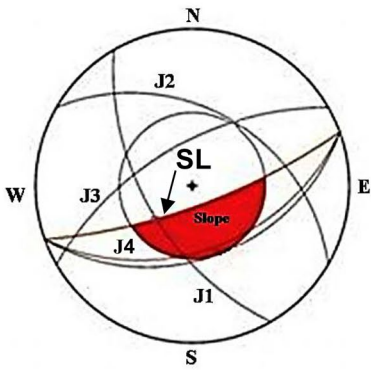
L4: Plane (J1), Wedge Failure



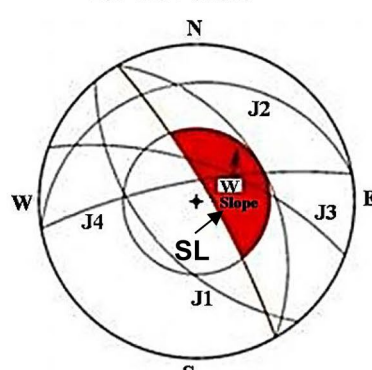
L5: No Failure



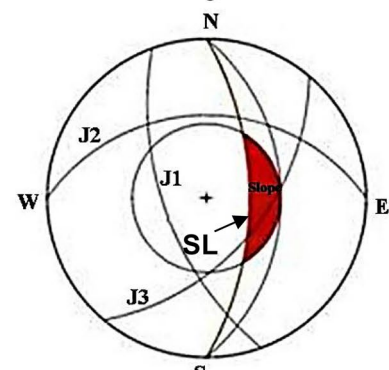
L6: Wedge Failure



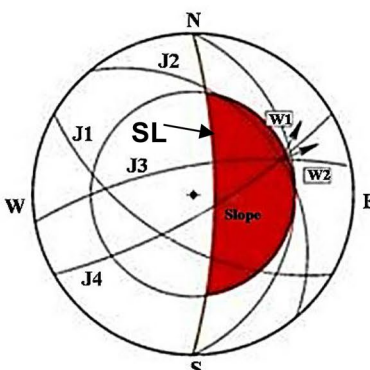
L7: Plane failure (J4), Toppling



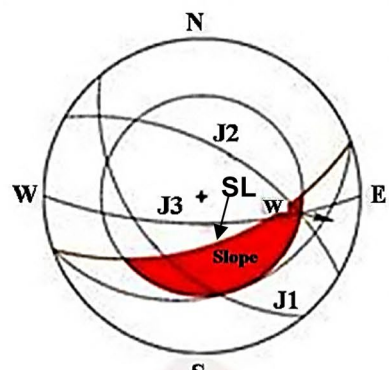
L8: Wedge Failure, Toppling



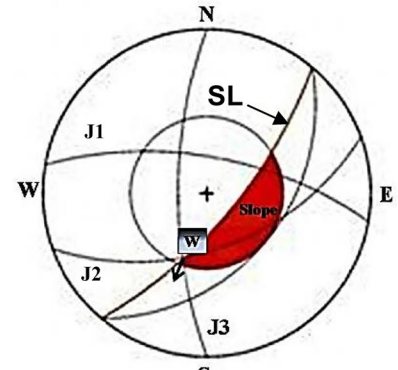
L9: Toppling



L10: Wedge Failure



L11: Wedge Failure



L12: Wedge Failure

Fig. 9 Stereographic projection plots of slope face (SL) and discontinuity sets (J1, J2, J3 etc.) for kinematic analysis of cut slopes in the studied section at locations L1 to L12 (see Fig. 1 for reference). The type of failure i.e. plane, wedge, toppling or any combinations thereof are also indicated for each location. The friction circle inside the plot is in accordance with the average friction angle of the discontinuities shown in Table 4

4.7 Rock Mass Rating (RMR_b)

Rock mass rating (Harrison and Hudson 2000), originally established by Bieniawski (1973, 1989) and herein referred to as RMR_b is defined as a comprehensive index of rock mass quality that is derived from cumulative weighted values of significant geological parameters of influence. The RMR system consists of five basic parameters that represent different conditions of the rock and discontinuities. These parameters are: (1) UCS of intact rock, (2) rock quality designation (RQD), (3) spacing of discontinuities, (4) condition of discontinuities and (5) groundwater. RMR_b is expressed as a rating score in the range of 0–100 (Bieniawski 1973, 1989) with higher values indicative of relatively better rock mass quality than those with lower values. RMR_b is widely used for tunnels, dam foundations and mines but strictly does not apply to slopes (Aksoy 2008). The guidelines for assigning rating scores for the parameters in RMR_b is provided in details by Bieniawski (1973, 1989). Based on rating scores, the RMR_b classifies Rock masses into five classes. They are Class-I (Very good rock, Rating 100–81), Class-II (Good rock, Rating 80–61), Class-III (Fair Rock, Rating 60–41), Class-IV (Poor rock, Rating 40–21) and Class-V (Very poor rock, Rating < 20).

In a recent development, a modified RMR_b has been proposed by Chen and Yin (2020) by introducing a Modified Blockiness Index in place of RQD, Joint frequency and Joint volume (J_v) parameters that are inherent within RMR_b of Bieniawski (1989). However, when RMR_{mbi} is plotted against RMR_b of Bieniawski (1989), the line of best fit closely conforms to the 1:1 line, meaning that the RMR_{mbi} cannot be distinguished from the original RMR_b in most of the cases (Fig. 28 of Chen and Yin 2020). Therefore, for the present study, the widely used and validated RMR_b (Bieniawski 1989) method is used for the road-cut slopes in the study area.

The RMR_b scores for all locations are presented in Table 5. The RMR_b of the road-cut slopes in the study area ranges between 55 and 78. The location L10 corresponds to RMR_b 55 and indicate a ‘fair rock’ category (Class-III). The rock mass of the remaining locations range between 61 and 80 and belong to the ‘good rock’ category (Class-II). The RMR_b is further used for estimating various slope mass rating parameters.

4.8 Modified Geological Strength Index (Modified GSI)

Strength of jointed rock masses is difficult to determine since the size of representative specimens is too large for laboratory testing. This restriction led to the development of practical methods, particularly empirical strength criteria, which can provide good estimate for the strength of closely jointed rock masses. Amongst the empirical strength criteria formulated both for intact rock and rock masses, the widely accepted and popular Hoek–Brown criterion (Hoek and Brown 1980) is used in conjunction with the Bieniawski’s RMR_b System (Bieniawski 1989) as an attempt to address the problem, and has been refined and expanded over the years (Hoek 1983, 1994; Hoek and Brown 1988; Hoek et al. 1992, 1995). It was also recognized that RMR_b was not fully appropriate for relating the failure criterion to geological observations in the field, particularly for very weak rock masses. This led to introduction of a new classification of rock masses termed as Geological strength Index (GSI) (Hoek et al. 1992, 1995; Hoek 1994; Hoek and Brown 1997). The GSI System is based upon the visual impression on the rock mass structure and has twenty codes to identify each rock mass category and estimates the GSI value ranging between 10 and 85. The GSI was subsequently extended for weak rock masses through a series of publications by Hoek et al. (1998), Marinis and Hoek (2000, 2001), Marinis et al. (2005).

However, due to lack of measurable and more representative parameters, and related interval limits or ratings for describing the surface conditions of the discontinuities, the GSI for each rock mass category in the chart proposed by Hoek and Brown (1997), represents a range of values. This implies that, it is possible to estimate different GSI values from the chart for the same rock mass by different persons, depending on their personal experience.

Therefore, an attempt has been made by Sönmez and Ulusay (1999) to provide a more quantitative numerical basis for evaluating the GSI and to suggest quantities that make more sense than that of the RMR_b System when used for the estimation of the rock mass strength.

The quantitative GSI System and associated approaches and input parameters for its construction are given by Sönmez and Ulusay (1999) in detail. The GSI was further modified by Sönmez and Ulusay (2002), herein referred to as Modified GSI, based on the structure and surface condition ratings, including five rock mass categories to provide a complete GSI rating scores ranging between 5 and 100 in the form of chart as illustrated in Fig. 11. Two important parameters that form the framework of modified GSI classification are Structure rating (SR) based on volumetric joint count and the Surface condition rating (SCR) based on roughness, weathering and infiltration characteristics.

Table 4 Kinematic analysis of slopes in the studied locations

Slope location	Slope orientation (dip/direction) (degrees)	Type of failure	Discontinuities involved (dip/direction in degrees) (joint set)	Friction angle (ϕ) (degrees)	Orientation of Wedge axis (plunge/plunge direction) (degrees)
L1	75/80	Wedge Topple	66/195 (J1), 40/145 (J3) 31/240 (J4)	35	38.4/125.6 –
L2	60/125	No failure	–	35	–
L3	60/120	Wedge Topple	55/195 (J2), 55/120 (J3) 51/330 (J1)	40	48.6/157.5 –
L4	80/90	Plane Wedge	47/118 (J1) 47/118 (J1), 60/230 (J3)	30	– 36.4/164
L5	80/90	No failure	–	35	–
L6	70/140	Wedge	50/240 (J1), 66/140 (J3)	40	44.1/204.4
L7	75/160	Plane Topple	43/160 (J4) 60/330 (J3)	40	–
L8	80/60	Wedge Topple	63/20 (J3), 75/350 (J4) 51/230 (J1)	40	58.4/54.2 –
L9	60/90	Topple	60/250 (J1)	40	–
L10	75/90	Wedge	30/50 (J2), 75/150 (J4)	25	28.7/68.4
L11	55/160	Wedge	55/30 (J2), 70/180 (J3)	25	25.9/100.2
L12	70/130	Wedge	52/160 (J2), 70/270 (J3)	40	44.1/200.7

From these values of SR and SCR, modified GSI can be estimated from the chart (Fig. 11). The modified GSI scores for the slopes of the studied locations are determined and presented in Table 6, where the input parameters correspond to the parameters in the modified GSI chart as described by Sönmez and Ulusay (2002).

The modified GSI scores for each slope locations are further plotted in the GSI chart to show their rock mass characteristics indicated on the left boundary (Fig. 11). The modified GSI values agrees closely with the GSI value range visually estimated in the field (Table 2). The modified GSI scores were further used as input parameters in other geomechanical classification of slopes as subsequently discussed.

4.9 Slope Mass Rating (SMR)

The RMR system of Bieniawski (1973, 1989), was mainly developed for tunnels, underground excavations and dam foundations but had limited use in assessing stability of slopes. To extend the use of RMR, Romana (1985), proposed a slope mass rating (SMR) classification system to characterize the quality of slopes. SMR is originally derived from RMR system and is expressed by the following equation:

$$\text{SMR} = \text{RMR} + (F_1 \times F_2 \times F_3) + F_4, \quad (1)$$

where F_1 , F_2 , F_3 and F_4 are factors that are defined as follows:

F_1 depends on the parallelism between dip-direction of the plane of discontinuity, α_j (for planar slides and topples) or the plunge azimuth of the line of intersection α_i , between two discontinuities (in case of wedge failure) and the dip-direction α_s of the slope.

F_2 depends on the dip amount β_j of the discontinuity in case of plane failure and the plunge β_i of the intersection line of two discontinuities in wedge failure. As regards toppling failure F_2 takes the value 1.0. This parameter is related to probability of discontinuity shear strength (Romana 1993).

F_3 depends on the relationship between dip amounts of slope β_s and discontinuity β_j (for toppling and planar failure cases) or plunge of line of intersection (β_i) of two discontinuity planes (wedge failure case). This parameter varies from 0 to –60 rating points and expresses the probability of discontinuity outcropping on the slope face (Romana 1993) for planar and wedge failures. For toppling failure this parameter varies from 0 to –25 rating points.

F_4 is the correction factor that depends on excavation method used to generate the cut slope and the rating value is selected empirically. The SMR of Romana (1985) was based on discrete functions and considered only planar and toppling-type failure modes. The SMR of Romana (1985) was subsequently modified by Anbalagan et al. (1992) (Table 7) by including an addition of wedge failure condition. This modified SMR (Table 7) is herein referred to as *original SMR* whose parameters and functions (A, B, and C) for assigning rating values are used in this study. Based on SMR scores, slopes can be classified as completely

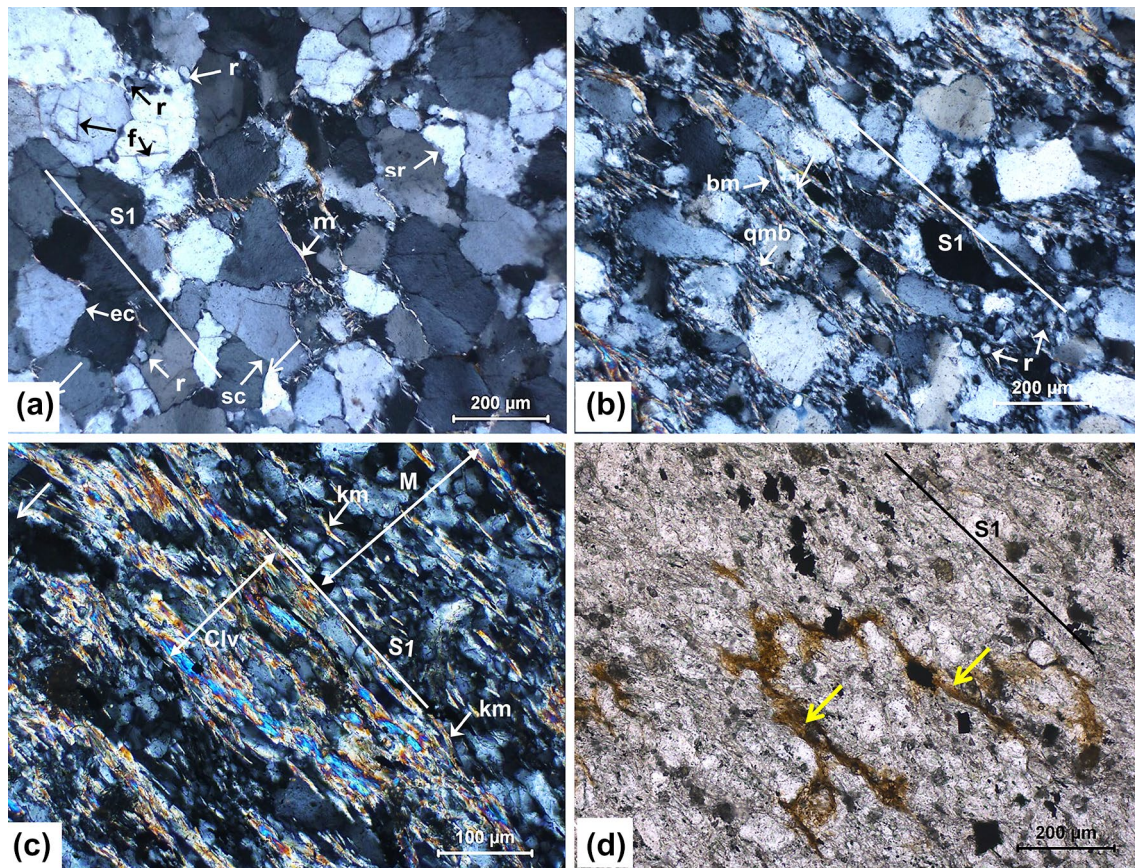


Fig. 10 Microstructures from oriented thin sections cut orthogonal to foliation and lineation of the representative lithounits of the study area. **a** Preferred orientation of grain boundaries parallel to the long dimensions of quartz grains, defines cleavage (S1) in White quartzites. Films and fine fibers of mica (m) are oriented parallel to S1. Abbreviations for quartz microstructures: sc—straight grain contact, sr—serrated grain contact, ec—embayed grain contact, r—dynamically recrystallized grains, f—fractures, CPL. **b** relatively higher volume percentage of phyllosilicates show a strong preferred dimensional orientation of mica defining S1 in schistose quartzites. Note that the cleavage defined by mica aggregates anastomose around the quartz grains with development of bent mica (bm) in the cleavage seams.

Quartz-mica beards (qmb) develop at the grain boundaries of detrital quartz grains that are orthogonal to the cleavage, CPL c Domainal cleavage (S1) defined by alternating bands (domains) of dominantly quartz grain aggregates as microlithons (M) and dominantly mica grain aggregates as cleavage domains (Clv) in phyllites. Mica grains exhibit kinking (km), CPL. (d) Locus of water movement (arrow) along foliation planes in phyllites, PPL. Brown stains are due to precipitation of ferruginous material during water circulation. Note that the brown stain zones are parallel to the rock cleavage, indicating seepage of water along cleavage (S1). CPL crossed polarized light, PPL plane polarized light

stable (81–100, Class-I), stable (61–80, Class-II), partially stable (41–60, Class-III), unstable (21–40, Class-IV), and completely unstable (0–20, Class-V), with corresponding probability of failure (Romana 1985; Romana et al. 2015) (Table 8). The input parameters for determining the original SMR is documented in Table 9.

The results of original SMR for all the locations are presented for structurally controlled slope failures in Table 10 that include wedge and toppling failure. The original SMR ranges between 16 and 62.90. Slopes at two locations viz. L8 and L10 that are marked by rating scores of 16 and 24.20 respectively get classified as completely unstable and unstable category respectively. Slopes at L3 and L6

get classified as stable whereas the other locations are partially stable.

4.10 Continuous Slope Mass Rating (Continuous SMR)

The discrete SMR functions of Romana (1985) were replaced by continuous functions for the parameters F_1 , F_2 and F_3 by Tomás et al. (2007) to propose the new system of continuous SMR. The new functions are expressed as follows:

Table 5 Determination of RMR_b of the slopes of the studied locations, based on the rating of various rock mass PARAMETERS

Slope location	Rock type	Rating of parameters of rock Mass characterization										RMR _b
		JCS	RQD	Water inflow	Joint spacing	Weathering	Joint persistence	Joint Aperture	Joint Roughness	Joint Filling		
L1	Schistose Quartzites with interbands of phyllite	12	13	15	8	5	1	1	1	3	6	64
L2	Quartzites with interbands of phyllite	12	13	15	8	5	1	1	1	3	6	68
L3	Light Gray Quartzites	15	17	15	10	5	1	1	1	3	6	73
L4	Light gray Quartzite	15	17	15	10	5	1	1	1	3	6	73
L5	White Quartzite	15	17	15	10	5	1	1	1	3	6	73
L6	Quartzites with interbands of phyllite	15	17	15	10	5	1	1	1	5	6	75
L7	White Quartzite and metavolcanics	12	17	15	10	5	1	1	1	6	6	73
L8	Quartzite	12	17	15	10	5	1	1	1	5	6	75
L9	Dark Gray Quartzite with interbeds of slate	12	17	15	10	5	1	1	1	6	6	73
L10	Phyllite with interbands of Quartzite	8	8	15	8	3	1	1	1	3	2	49
L11	Schistose Quartzite	12	13	15	8	5	1	1	1	3	6	64
L12	Dark Gray Quartzite	12	13	15	10	5	1	1	1	3	6	66

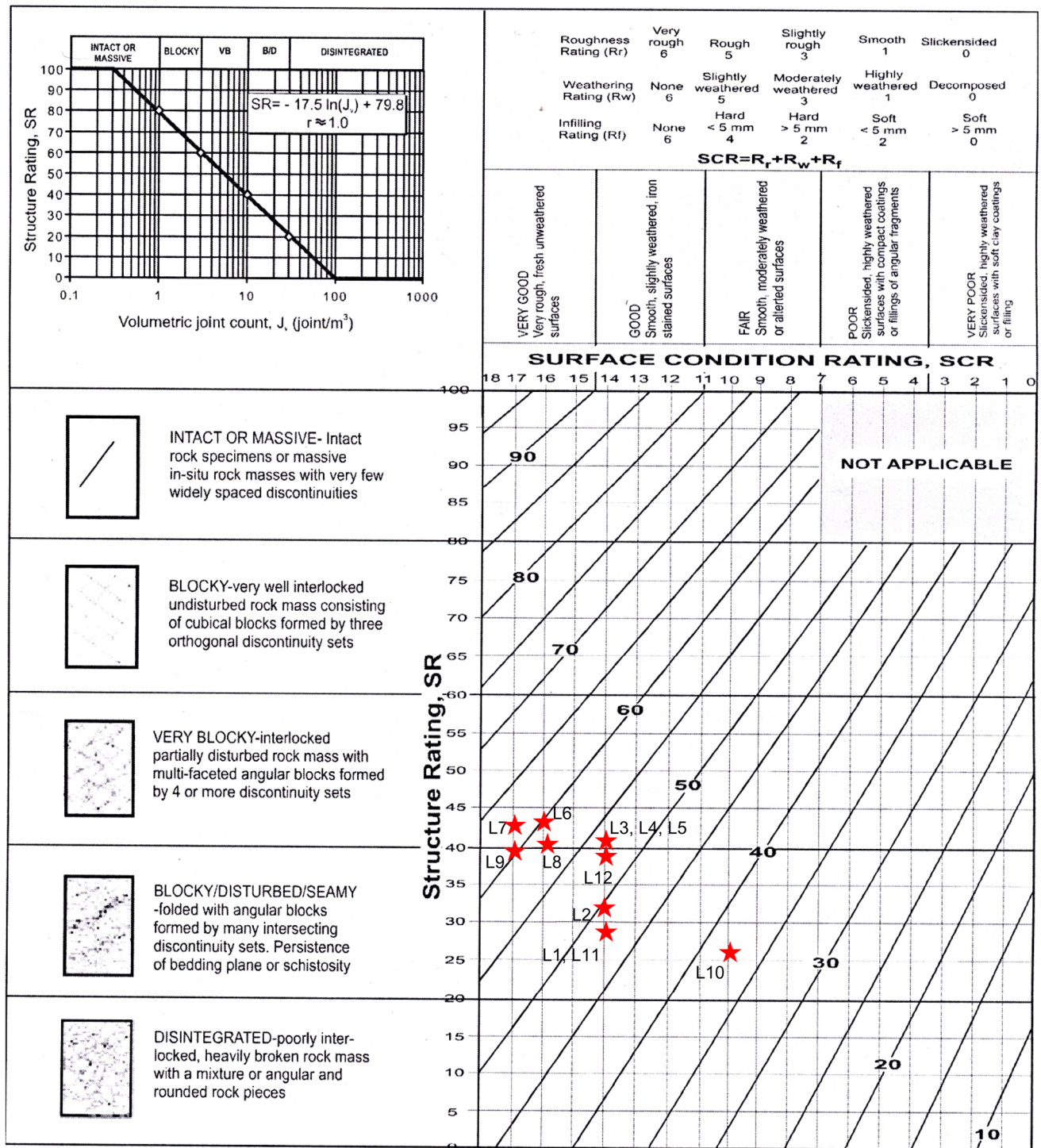


Fig. 11 Plot of Modified GSI values of the slopes of the studied locations on the modified GSI chart designed by Sonmez and Ulusay (2002)

$$F_1 = \frac{16}{25} - \frac{3}{500} \arctan \left[\frac{1}{10} (|A| - 17) \right],$$

(2)

where, $|A| = |\alpha_j - \alpha_s|$ for plane failure, $|A| = |\alpha_j - \alpha_s - 180^\circ|$ for toppling failure and $|A| = |\alpha_i - \alpha_s|$ for wedge failure. α_j and α_s are, respectively, the dip directions of the joint and slope. α_i is the plunge direction of the line of intersection of two planes defining the wedge.

Table 6 Determination of Modified Geological Strength Index (GSI) of the slopes in the studied locations

Slope Location	J_v	R_r	R_w	R_f	SCR	SR	Modified GSI
L1	18	3	5	6	14	29.21	48.30
L2	15	3	5	6	14	32.41	50.00
L3	9	3	5	6	14	41.34	53.50
L4	9	3	5	6	14	41.34	53.50
L5	9	3	5	6	14	41.34	53.50
L6	8	5	5	6	16	43.40	59.50
L7	8	6	5	6	17	43.40	64.50
L8	9	5	5	6	16	41.34	58.30
L9	10	6	5	6	17	39.50	60.50
L10	21	5	3	2	10	26.52	38.25
L11	18	3	5	6	14	29.21	48.30
L12	10	3	5	6	14	39.50	52.50

Table 7 Adjustment ratings for F_1, F_2, F_3 (modified from Romana (1985) by Anbalagan et. al. (1992)) and F_4 (Romana 1985). A, B, and C are functions for assigning rating values to factors F_1, F_2 and F_3 respectively

Type of failure			Very favorable	Favorable	Fair	Unfavorable	Very unfavorable
P	A	$ \alpha_j - \alpha_s $	$> 30^\circ$	$30-20^\circ$	$20-10^\circ$	$10-5^\circ$	$< 5^\circ$
T		$ \alpha_j - \alpha_s - 180 $					
W		$ \alpha_i - \alpha_s $					
$P/T/W$ (Rating)	F_1		0.15	0.40	0.70	0.85	1.00
P/W	B	$ \beta_j $ or $ \beta_i $	$< 20^\circ$	$20-30^\circ$	$30-35^\circ$	$35-45^\circ$	$> 45^\circ$
P/W (Rating)	F_2		0.15	0.40	0.70	0.85	1.00
T (Rating)			1.00				
P	C	$\beta_j - \beta_s$	$> 10^\circ$	$10-0^\circ$	0°	$1 - (-10^\circ)$	$< (-10^\circ)$
W		$\beta_i - \beta_s$					
T		$\beta_j + \beta_s$	$< 110^\circ$	$110-120^\circ$	$> 120^\circ$	–	–
$P/T/W$ (Rating)	F_3		0	-6	-25	-50	-60

Excavation Method (F_4) (Rating as indicated below):

Natural Slope: +15, Pre-splitting: +10, Smooth Blasting: +8, Normal Blasting or Mechanical Excavation: 0, Deficient Blasting: -8

P : planar sliding, W : wedge sliding, T : toppling

The factors and their ratings are shown in bold

Table 8 Description of SMR Classes (Romana 1985)

Class	SMR	Description	Stability	Failure probability
I	81-100	Very Good	Completely stable	0.0
II	61-80	Good	Stable	0.2
III	41-60	Normal	Partially stable	0.4
IV	21-40	Bad	Unstable	0.6
V	0-20	Very bad	Completely unstable	0.9

where, B (measured in degrees) is the magnitude of dip of joint for planar and toppling failure modes i.e. β_j and the magnitude of plunge β_i of the line of intersection of two planes for wedge-type failure.

$$F_3 = -30 + \frac{1}{3} \arctan C. \tag{4}$$

$$F_3 = -30 + \frac{1}{3} \arctan(C - 120), \tag{5}$$

where C (in degrees) is defined as follows:

$$F_2 = \frac{9}{16} - \frac{1}{195} \arctan \left[\frac{17}{100} B - 5 \right]. \tag{3}$$

- (1) The difference in angle between the dip amounts of joint and slope i.e. $(\beta_j - \beta_s)$ for planar- type failure mode;

- (2) The difference in angle between the plunge amount of the line of intersection of two planes and the dip amount of the slope, i.e. $(\beta_i - \beta_s)$ for wedge-type failure mode;
- (3) The sum of the two dip amounts of joint and slope i.e. $(\beta_j + \beta_s)$ for toppling-type failure mode.

Equation (4) is used for slopes with planar -or wedge-type failure mode and Eq. (5) is used for slopes with toppling-type failure mode. The input parameters for determining the continuous SMR as applicable to the slopes whose failures are structurally controlled are presented in Table 9. The results of continuous SMR of the slopes for wedge failure and toppling failure are presented in Table 10. The continuous SMR varies between 14.17 and 64.68. Slopes at location L8 with rating 14.17 and location L10 with rating 22.69 get classified as completely unstable and unstable respectively. The slopes of location L3 and L4 are stable whilst the slopes of the remaining locations belong to partially stable category.

4.11 Chinese Slope Mass Rating (CSMR)

Chinese slope mass rating (CSMR) system was proposed by Chen (1995) and is a modification of the SMR of Romana (1985), whereby it introduces two new components to Romana’s SMR system. These are the slope

height factor (ζ) and the discontinuity factor (λ) as follows:

$$CSMR = \zeta RMR + \lambda F_1 F_2 F_3 + F_4. \tag{6}$$

where ζ is a non-dimensional parameter that accounts for the effect of slope height and is given by $\zeta = 0.57 + 0.43 \times (80/H)$, where H is the slope height in meters. λ is a parameter accounted for the effect of discontinuity type and is defined as follows:

- (1) $\lambda = 1$ for faults of long weak seams filled with clay;
- (2) $\lambda = 0.8-0.9$ for bedding planes of large-scale joints with gouge and
- (3) $\lambda = 0.7$ for joints of tightly interlocked bedding planes.

F_1, F_2, F_3 and F_4 are the same factors of the original SMR. Regarding the slope height, Eq. (6) is applicable when slope height H exceeds 80 m. For $H < 80$ m, $\zeta = 1$. The CSMR rating scores for all the slopes whose failure is structurally controlled is presented in Table 10 for wedge and toppling failure. CSMR scores of the study area range between 31.3 and 63.32. Locations L8 and L10 have scores of 31.3 and 29.24 respectively and both belong to unstable category. Locations L3, L4 and L6 belong to stable and the remaining locations belong to partially stable category.

Table 9 Input parameters for determining SMR, CSMR and Chinese SMR in the slopes of the studied locations

Slope Location	Type of Failure	Slope Orientation (degrees)		Orientation of Discontinuity planes/wedge axis (degrees)		Functions for Adjustment factors (degrees)		
		α_s	β_s	α/α_i	β/β_i	A	B	C
L1	Wedge	80	75	125.6	38.4	45.6	38.4	-36.6
	Topple	80	75	240	31	20	31	106
L2	Non structurally controlled	125	60	-	-	-	-	-
L3	Wedge	120	60	157.5	48.6	37.5	48.6	-11.4
	Topple	120	60	330	51	30	51	111
L4	Plane	90	80	118	47	28	47	-33
	Wedge	90	80	165.6	36.9	75.6	36.9	-43.1
L5	Non structurally controlled	90	80	-	-	-	-	-
L6	Wedge	140	70	204.4	44.1	64.4	44.1	-25.9
L7	Plane	160	75	160	43	0	43	-32
	Topple	160	75	330	60	10	51	131
L8	Wedge	60	80	54.2	58.4	5.8	58.4	-21.6
	Topple	60	80	230	51	10	51	131
L9	Topple	90	60	250	60	20	60	120
L10	Wedge	90	75	70	30	20	30	-46
L11	Wedge	60	55	100	26	60	26	-29
L12	Wedge	130	70	200	44	70	44	-26

Table 10 Determination of various slope mass rating scores of adjustment factors determined from respective functions, for the slopes of the studied locations

Slope location	Type of failure	RMR	Original SMR					Continuous SMR					Chinese SMR		
			F1	F2	F3	F4	Score	F1	F2	F3	F4	Score	ζ	λ	Score
L1	Wedge	64	0.15	0.85	-60	-8	48.35	0.21	0.85	-59.47	-8	45.18	1	0.7	53.88
	Topple		0.70	1.00	0	-8	56.00	0.54	0.64	-0.73	-8	55.74	1	0.7	56.00
L2	Non structurally controlled	68	-	-	-	-	-	-	-	-	-	-	-	-	-
L3	Wedge	73	0.15	1.00	-60	-8	56.00	0.26	0.94	-58.32	-8	51.02	1	0.7	58.70
	Topple		0.40	1.00	-6	-8	62.60	0.32	0.95	-1.05	-8	64.68	1	0.7	63.32
L4	Plane	73	0.40	1.00	-60	-8	41.00	0.35	0.93	-59.42	-8	46.02	1	0.7	51.71
	Wedge	73	0.15	0.85	-60	-8	57.35	0.16	0.83	-59.50	-8	57.09	1	0.7	59.55
L5	Non structurally controlled	73	-	-	-	-	-	-	-	-	-	-	-	-	-
L6	Wedge	75	0.15	0.85	-60	-8	59.35	0.17	0.91	-59.20	-8	57.84	1	0.7	61.64
L7	Plane	73	1.00	0.85	-60	-8	14.00	0.99	0.90	-59.40	-8	12.07	1	0.7	29.30
	Topple	73	0.85	1.00	-25	-8	43.75	0.85	0.96	-25.30	-8	44.35	1	0.7	50.12
L8	Wedge	75	0.85	1.00	-60	-8	16.00	0.93	0.96	-59.11	-8	14.17	1	0.7	31.30
	Topple		0.85	1.00	-25	-8	45.75	0.85	0.96	-25	-8	47.02	1	0.7	52.12
L9	Topple	73	0.70	1.00	-25	-8	47.50	0.85	0.97	-19.40	-8	49.00	1	0.7	52.75
L10	Wedge	49	0.40	0.70	-60	-8	24.20	0.54	0.60	-59.57	-8	22.69	1	0.7	29.24
L11	Wedge	64	0.15	0.40	-60	-8	52.40	0.18	0.41	-59.34	-8	51.66	1	0.7	53.48
L12	Wedge	66	0.15	0.85	-60	-8	50.35	0.16	0.98	-59.26	-8	48.39	1	0.7	52.64

4.12 Q-Slope Rating

The Q- slope system stemmed out from the necessity and tendency of applying to slopes the widely accepted Q-system of rock mass classification that was originally developed for tunnels (Barton et al. 1974). The original Q-system is a quantitative classification system for estimates of tunnel support, based on a numerical assessment of the rock mass quality using the following six parameters:

1. Rock quality designation (RQD).
2. Number of joint sets (J_n).
3. Roughness of the most unfavorable joint or discontinuity (J_r).
4. Degree of alteration or filling along the weakest joint (J_a).
5. Water inflow (J_w).
6. Stress condition given as the stress reduction factor (SRF); composed of:
 - (a) Loosening load in the case of shear zones and clay bearing rock,
 - (b) Rock stress in competent rock, and
 - (c) Squeezing and swelling loads in plastic, incompetent rock.

The above six parameters are grouped into three quotients to give the overall rock mass quality as follows:

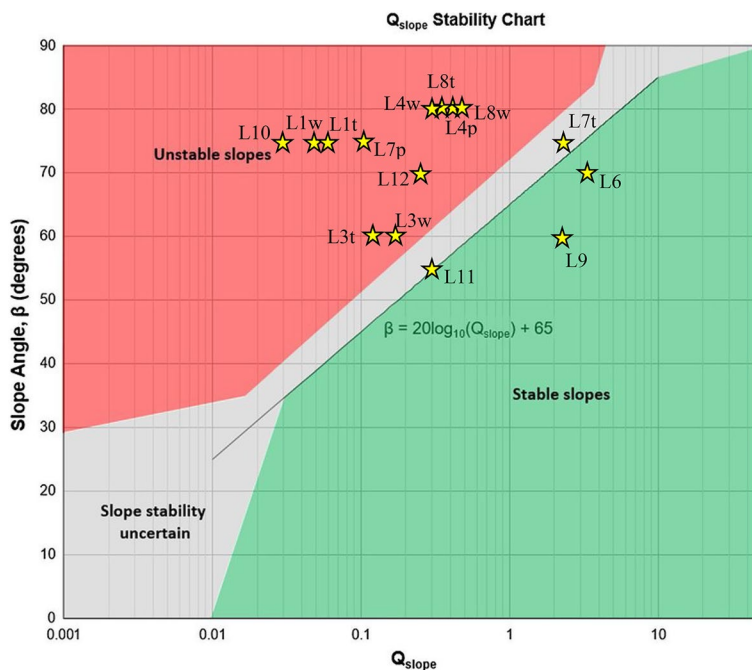
$$Q = \frac{RQD}{J_n} \times \frac{J_r}{J_a} \times \frac{J_w}{SRF} \quad (7)$$

- i. The first two parameters represent the overall structure of the rock mass, and their quotient is a relative measure of the block size.
- ii. The second quotient is described as an indicator of the inter-block shear strength.
- iii. The third quotient is described as the “active stresses”.

However, the Q-system was not applicable to slopes. To extend the application of Q-system of geomechanical classification to slopes, Bar and Barton (2015) proposed the new Q-slope classification system.

Q-slope is an empirical rock slope engineering method for assessing the stability of excavated rock slopes in the field. Intended for use in reinforcement-free road or railway cuttings or in opencast mines, Q-slope allows potential adjustments to be made to slope angles as rock mass conditions become apparent during construction. Through worldwide case studies, a simple correlation between Q-slope and long-term stable slopes was established. Q-slope was developed by supplementing the Q-system

Fig. 12 Plot of Q-slope values of the slopes of the studied locations against their existing slope angles (p- plane, w-wedge, t-topple)



which has been extensively used for characterizing rock exposures, drillcore, and tunnels under construction for several decades (Barton and Grimstad 2014). The parameters RQD, J_n , J_a , and J_r in original Q-system remain unchanged in Q-slope. However, a new method for applying J_r/J_a ratios to both sides of potential wedges (in case of wedge failure indications), is used, with relative orientation weightings for each side. The term J_w , is replaced with J_{wice} that accounts for long-term exposure of slopes to various climatic and environmental conditions such as intense erosive rainfall and ice-wedging effects. Slope-relevant SRF categories for slope surface conditions, stress-strength ratios, and major discontinuities such as faults, weakness zones, or joint swarms have also been incorporated (Tables 7 and 8 of Bar and Barton 2017). Q-slope method is applicable to slopes ranging from less than 5 m to more than 250 m in height and is therefore applicable to the slope locations of the present study.

The Q-slope method requires the assignment of ratings for rock quality designation (RQD), joint set number (J_n), joint roughness number (J_r), and joint alteration number (J_a), from the Q-system (Barton et al. 1974). The formula for estimating Q-slope is as follows:

$$Q = \frac{RQD}{J_n} \times \left(\frac{J_r}{J_a} \times O \right) \times \frac{J_{wice}}{SRF_{slope}} \tag{8}$$

where, O is the Discontinuity orientation factor. As with the Q-system, the rock mass quality in Q-slope can be

considered a function of three parameters, which are crude measures of:

1. Block size: (RQD/J_n) .
2. Shear strength: least favorable (J_r/J_a) or average shear strength in the case of wedges $(J_r/J_a)1 \times (J_r/J_a)2$.
3. External factors and stress: (J_{wice}/SRF_{slope}) .

Shear resistance, τ , is approximated using:

$$\tau \approx \sigma_n \tan^{-1} \left(\frac{J_r}{J_a} \right) \tag{9}$$

The Q-slope ratings for rock quality designation, RQD (Deere 1963; Deere et al. 1967), joint set number (J_n), joint roughness number (J_r), and joint alteration number (J_a) remain unchanged from the Q-system (Barton et al. 1974; Barton and Bar 2015). The discontinuity orientation factor (O-factor) described in Table 5 of Barton and Bar (2017) provides orientation adjustments for discontinuities in rock slopes.

The environmental and geological condition number, J_{wice} , is more sophisticated than J_w of the original Q-system, since slopes are outside and exposed to the elements of weathering for a long time and includes tropical rainfall, erosion effects and ice-wedging effects (Table 6 of Bar and Barton 2017). Adjustment factors in case of slope reinforcement or drainage measures are also included.

Based on the evaluation of the parameters of Eq. (8), the slopes can be classified as stable or unstable when related between the Q-slope score of the slope in question and

Table 11 Determination of Q- Slope scores and safe slope angles in the studied locations

Slope location	RQD (%)	J_n	Unstable plane/line orientation (degrees)	Type of failure	Set A orientation (degrees)	Set B Orientation (Degrees)	Set A		Set B		O-factor		J_{wice}	SRF _{slope}	Q-Slope	Safe slope angle (degrees)
							J_r	J_a	J_r	J_a	Set A	Set B				
L1	55.6	15	38.4/125.6	Wedge	40/145	66/195	1.0	2.0	1.0	2.0	0.75	0.9	0.5	5	0.06	40.5
L2	62.2	15	31/240	Topple	31/240	-	1.0	2.0	-	-	0.25	-	0.5	5	0.05	38.9
L3	85.3	9	-	No Failure	55/120	55/195	1	2	1	2	0	1	0	2.5	0.1	49.9
L4	85.3	5	48.6/15	Wedge	51/330	-	5	0	0	0	25	0	5	2.5	7	46.4
L5	85.3	15	7.5	Topple	47/118	-	0.5	2.0	-	-	0.25	-	0.5	2.5	0.12	57.5
L6	88.6	9	51/330	Plane	47/118	-	1.0	2.0	-	-	0.75	-	0.5	2.5	0.42	54.0
L7	75.2	15	47/118	Wedge	47/118	60/230	1.0	2.0	1.5	2.0	0.75	0.9	0.5	2.5	0.28	-
L8	85.3	15	36.9/165.6	No Failure	45/200	50/240	1.5	1.0	1.5	1.0	0.75	1.0	0.5	2.5	3.32	75.4
L9	88.6	9	44.1/204.4	Wedge	43/160	-	1.0	2.0	-	-	0.25	-	0.5	2.5	0.12	46.5*
L10	45.7	15	43/160	Topple	60/330	-	1.5	1.0	-	-	0.75	-	0.5	2.5	1.12	66.0
L11	55.6	9	60/330	Wedge	63/20	75/350	1.0	2.0	1.5	1.0	0.75	0.9	0.5	3.0	0.48	58.6
L12	55.6	9	58.4/54.2	Topple	51/230	-	1.5	2.0	-	-	0.50	-	0.5	3.0	0.35	56.0
L9	88.6	9	51/230	Topple	60/250	-	3.0	2.0	-	-	0.75	-	0.5	2.5	2.21	71.9
L10	45.7	15	60/250	Wedge	30/50	75/150	1.0	3.0	1.5	3.0	0.75	1.0	0.5	7	0.03	34.5
L11	55.6	9	28.7/68.4	Wedge	70/270	52/160	1.0	2.0	1.5	2.0	0.75	0.9	0.5	5	0.31	54.9
L12	55.6	9	25.9/100.2	Wedge	52/160	70/270	1.5	2.0	1.0	2.0	0.75	0.9	0.5	3	0.26	53.3
L12	55.6	9	44.1/200.7	Wedge	52/160	70/270	1.5	2.0	1.0	2.0	0.75	0.9	0.5	3	0.26	53.3

*Ideally it should be 43° and therefore it is in close approximation

Table 12 Rating criteria and scores for the subfactors used for quantification of f_{NC} (after Pantelidis (2010))

f_n	Failure hazard subfactors	Rating Criteria and score			
		1	3	6	10
f_1	Safety factor, F	2.0	1.5	1.25	≤ 1.0
f_2	$ \alpha_d - \alpha_s $	$\geq 40^\circ + \Delta\alpha$	$30^\circ + \Delta\alpha$	$20^\circ + \Delta\alpha$	$\leq 10^\circ + \Delta\alpha$
f_3	GSI	≥ 90	80	65	≤ 45
f_4	Volume of suspended rock mass per one-meter slope length	0.25 m^3	0.5 m^3	1.0 m^3	$\geq 2.0 \text{ m}^3$

$\Delta\alpha = 0^\circ, 20^\circ, 30^\circ$ or 40° for planar slides in rock masses that belong to the R3 (or greater), R2, R1 and R0 Wall Strength Grade class (Brown, (1981)), respectively. $\Delta\alpha = 10^\circ$ for flexural and block toppling (default value)

the existing slope angle or slope dip in the form of a chart (Fig. 12). The Q-slope scores for the slopes of each location in the study area are determined and the results are presented in Table 11. The scores are plotted on the Q-slope stability chart to show their stability when their existing slopes are considered (Fig. 12).

One important aspect of Q-slope classification is the prediction of safe slope angles based on the Q-slope scores. Barton and Bar (2017) provided equations for four categories of probability of failure (PoF) namely 1% PoF, 15% PoF, 30% PoF and 50% PoF. They are as follows:

$$\text{PoF 1\% : } \beta = 20 \log_{10} Q_{\text{slope}} + 65^\circ \tag{10}$$

$$\text{PoF 15\% : } \beta = 20 \log_{10} Q_{\text{slope}} + 67.5^\circ \tag{11}$$

$$\text{PoF 30\% : } \beta = 20 \log_{10} Q_{\text{slope}} + 70.5^\circ \tag{12}$$

$$\text{PoF 50\% : } \beta = 20 \log_{10} Q_{\text{slope}} + 73.5^\circ \tag{13}$$

In the present study the safe slope angle β with 1% PoF is considered from Eq. (10). The safe slope angles are presented against each slope locations that have structurally controlled failure in the last column of Table 11. From the plots in the Q-slope stability chart (Fig. 12) it can be observed that L1, L3, L4, L8, L10 and L12 are presently unstable slopes, and L9, L6 are stable slopes. The condition of L11 and L7 are quasi-stable with uncertainty.

4.13 Hazard Index

An alternative rock mass classification system for rock slopes in terms of rating scores that define a Hazard Index (HI) was proposed by Pantelidis (2010). The failure hazard of rock slopes is quantified in the form of rating tables where two separate functions are combined to give the hazard index. These are (1) function for normal (drained) condition of rock cutting, denoted as f_{NC} and (2) function for triggering mechanism for failure, denoted as f_{TM} . This model

of rock mass classification of slopes strongly considers the action of water in slope failure in addition to other factors and also applies to both structurally and non-structurally controlled slope failures. Since the study area experiences heavy rainfall during the monsoons (Fig. 2) and rock slopes in the study area are susceptible to triggering of failure by water including the two slope locations L2 and L5 whose instability is not structurally controlled, this classification is well applicable for the present study.

The f_{NC} is obtained from a combination of one or two out of four subfactors listed in Table 12. Each of these subfactors is rated according to pre-determined quantitative criterion on a scale from 1 to 10, including intermediate scores if required. Subfactor f_1 applies only to the structurally controlled failure (planar and wedge slides and topples) and is largely based on the apparent shear strength of the discontinuities. Subfactor f_2 is used only in the case of planar and toppling failure and refers to the relative orientation of the dominant failure planes with respect to the slope face ($\alpha_d - \alpha_s$) where α_d and α_s are strikes of the discontinuity plane and slope face respectively. For planar slides and flexural and block topples, Pantelidis (2010) showed that:

$$f_{NC} = 0.1f_1f_2 \tag{14}$$

For wedge slides and toppling of individual blocks:

$$f_{NC} = f_1 \tag{15}$$

Subfactors f_3 and f_4 applies to non-structurally controlled slope failures and are related to the GSI and differential weathering respectively. The GSI is based on assessment of lithology, structure and conditions of discontinuity in rock mass. Here the modified GSI values of the slope locations as determined earlier have been used. Differential weathering refers to the weight of the exposed unsupported (due to undercutting by preferentially weathering of weaker rocks) rock mass per one-meter length of slope. The stability conditions of an undercut slope under drained conditions is given by:

$$f_{NC} = (f_3 f_4)^{0.5} \quad (16)$$

If there is no undercutting by differential weathering and the slope has a non-structurally controlled failure that includes rock mass containing randomly oriented discontinuities but behaves as if it were isotropic, or excavations with a loose surface (e.g. due to inefficient blasting) or highly weathered rock slope masses, then the stability of such slopes under drained conditions is given by:

$$f_{NC} = f_3 \quad (17)$$

The quantitative attribution of the triggering mechanism (f_{TM}) is specified by the influence of surface and groundwater (drainage factor f_D) and the ratio of the mean annual precipitation to the critical annual precipitation against the stability behavior of the rock slope. Drainage factor f_D is obtained by field observation of the slope materials and the structures of the rock slopes and subsequently by assigning scores (1, 3, 6 or 10) (Pantelidis 2010) as described in Table 13.

The final score of the triggering mechanism f_{TM} is obtained by the product of the score of drainage factor f_D and the ratio of mean annual precipitation to the critical annual precipitation as follows:

$$f_{TM} = \frac{I_m}{I_{cr}} f_D \quad (18)$$

where I_m is the mean annual precipitation, I_{cr} is the critical annual precipitation height ($I_{cr} = 700$ mm, fixed conservative value) and f_D is the drainage factor. If $I_m > I_{cr}$ then the ratio $(I_m/I_{cr}) = 1$ in Eq. 11 (Pantelidis 2010). In studied slope locations, $I_m = 761.31$ mm (Sect. 2.3, Fig. 2) and is therefore greater than I_{cr} . Therefore, in the study area $(I_m/I_{cr}) = 1$.

The hazard index (HI) is expressed as follows:

$$HI = (f_{NC} \times f_{TM})^{\frac{1}{2}} \quad (19)$$

HI is given on a scale of 1–10 defining four intervals, i.e., 1–4 (good), 4–6 (fair), 6–8 (poor) and 8–10 (very poor). The HI for the slopes of all the twelve locations in the studied road-cut section is presented for both structurally controlled and non-structurally controlled failure in Table 14. The HI in the study area range between 2.19 and 8.9 and correspond to good to very poor category. For wedge failure, HI varies between 3.46 and 8.94 corresponding to the range of good to very poor category (Table 14). Location L8 gets classified as very poor and L11 as good category. The remaining locations belong to poor category as shown in Table 14. For toppling failure, the HI range is 2.19–8.94 (Table 4) and therefore ranges between good and very poor category. L1 and L3 belong to good, L9 is of fair, and L7, L8 are of very poor category.

For non-structurally controlled slopes, L2 belongs to poor and L5 to very poor category.

5 Discussions

5.1 Identification of Unstable Slopes

From geological field investigations and from the several slope mass rating classifications, locations L7, L8 and L10 are considered to be highly prone to failure. In these locations the road is ~ 6 m wide and the slope height is between 26 and 30 m (Table 2). Since the slope height is several times larger than the road width, failure along ‘day-lighted’ discontinuity surfaces or wedge axis on the slope face at the base of the slope, can translate large volumes of hanging wall materials (debris) on to the road. The debris materials can effectively block the road and can even overshoot the road to the adjoining slope of the Bhagirathi River valley, similar to what is observed in Fig. 6c, d. The slope height and the road width are therefore important parameters to be taken into account during design of safe cut slopes. Figure 13 illustrates the probabilities of failure for the structurally controlled slopes. As can be seen from Fig. 13a, the probability of planar failure in L7 and wedge failure in L8 is 0.9 and that of L10 is 0.8. The slopes at L8 and L10 therefore require immediate mitigation. The probability of failure by toppling (Fig. 13b) in these two slopes is relatively lower. It has been particularly observed in the field, that slopes at L7 (Fig. 7a) and L8 (Fig. 6a) have failed to a large extent, exactly in accordance with kinematic predictions.

Two slopes, L2 and L5 show no structurally controlled failure potentiality as indicated by kinematic analysis (Fig. 9) but are marked by poor GSI values and poor to very poor HI (Table 14). These slopes are therefore considered potentially hazardous too, especially during monsoons. Slope failure, if occurs in these locations, can initiate even from natural slope portions that overlook the cut slopes and may be shallow circular type and would resemble that of failures illustrated in Fig. 6c, d. Cut slopes of locations other than those mentioned above in the study area and those that are evaluated as partially stable, need to be under careful monitoring and surveillance.

5.2 Proposition of New Stability Charts

Several geomechanical classification systems applied to slopes have been used in this study for slope stability assessment. Since the parameters chosen in each of these classification systems vary from one another, slopes classified as stable or partially stable in one system may appear as unstable in others and vice-versa. For example, slopes at L1 appear to be partially stable when classified

Table 13 Rating criteria and scores for the drainage subfactors f_D (after Pantelidis (2010))

Drainage subfactors	Rating criteria and score				
	1	3	6	10	
Underground water Case-1					<i>Unfavorable conditions</i>
a. Potential for water infiltration from the upslope area, $f_{D, 1a}$	<i>Favorable conditions</i> Mantle: Impermeable Upslope Gradient: Abrupt Coverage: The upslope area is covered by dense evergreen forest or urban development Water circulation seems impossible (very tight or hard-filled discontinuities or intact rock)	Two favorable and one unfavorable condition are fulfilled -or- One favorable and two intermediate conditions are fulfilled Free drained cutting (wide unfilled discontinuities)	One favorable and two unfavorable conditions are fulfilled -or- One unfavorable and two intermediate conditions are fulfilled (I) fair drainage of underground water through unfilled or soft-filled discontinuities -and- (III) No or short freezing periods	Mantle: permeable Upslope gradient: gentle Coverage: The upslope area is bare or almost bare (e.g., sparse vegetation deciduous development) (II) Poor drainage of underground water through narrow unfilled or soft-filled discontinuities (IV) Long freezing periods	
b. Potential for build-up of hydrostatic pressures, $f_{D, 1b}$					
Surface water Case-2					
c. Potential for water inflow through exposed discontinuities and build-up of hydrostatic pressures, $f_{D, 2}$	Surface water flow is unlikely to trigger the type of failure studied (Water inflow seems impossible: very tight or hard-filled discontinuities or intact rock)	Minor inflow which can be drained through narrow discontinuities -or- Free drained cutting (wide unfilled discontinuities)	(I) Fairly drained rock mass with regards to the expected inflow quantity -and- (III) No or short freezing periods Instabilities are likely due to wash-out of infilling material	(II) Fairly drained rock mass with regards to the expected inflow quantity -and- (IV) Long freezing periods Major instabilities are likely due to wash-out of infilling material -or- A large amount of water flowing from upslope (e.g., from ravine) may cause the transportation of several loose blocks or stones	
d. Instabilities due to surface water flow, $f_{D, 3}$	Surface water flow is unlikely to trigger the type of failure studied (no loose stones or blocks, insignificant surface water flow etc.)	Minor instabilities are likely due to wash-out of infilling material -or- Water flow from upslope may cause the instability of only some small loose stones	Instabilities are likely due to wash-out of infilling material -or- Water flow from upslope may cause the transportation of a few loose blocks or stones		

The words “or” and “and” are used as logical operators

Intermediate scores are allowed in Case 1a (e.g., if the total of the three conditions regarding mantle, upslope gradient, and vegetation are neither favorable nor unfavorable then the rating value equals 4.5, if two of the conditions are unfavorable and one neither favorable nor unfavorable then the rating value equals 8)

The rating criteria of the last two columns of Case 1b and 2c can be combined, that is, (I) with (IV) and (II) with (III), giving a score equal to 8

If underground water is unlikely to trigger a failure incident, the drainage subfactors $f_{D, 1a}$ and $f_{D, 1b}$ equal unity

f_D is determined by the condition: $f_D = \max\{(f_{D, 1a} \times f_{D, 1b})^{0.5}, f_{D, 2}, f_{D, 3}\}$ (Pantelidis (2010))

Table 14 Determination of scores for Hazard Index (HI) from the rating values of the adjustment factors for the slopes in the studied locations

Slope locations	Type of failure	Normal (drained conditions of rock cutting)										Triggering mechanisms for failure			Hazard Index (HI)
		F	f_1	$ \alpha_d - \alpha_s $	f_2	GSI	f_3	Volume of suspended rock mass per one-meter slope length	f_4	f_{NC}	I_m/I_{cr}	f_D	f_{TM}		
L1	Wedge	1.22	6	-	-	-	-	-	-	-	6	1	8	8	6.92
L2	Topple	2.50	1	20°	10	-	-	-	-	-	1	1	8	8	2.82
L3	Non structurally controlled	-	-	-	-	50	6	-	-	-	6	1	8	8	6.92
L3	Wedge	0.83	10	-	-	-	-	-	-	-	10	1	8	8	8.94
L4	Topple	2.18	1	30°	6	-	-	-	-	-	0.6	1	8	8	2.19
L4	Plane	0.53	10	28°	4	-	-	-	-	-	4	1	6	6	4.80
L4	Wedge	0.95	10	-	-	-	-	-	-	-	10	1	6	6	7.74
L5	Non structurally controlled	-	-	-	-	53.5	-	-	-	-	8	1	8	8	8.00
L6	Wedge	1.14	7	-	-	-	-	-	-	-	7	1	6	6	6.48
L7	Plane	0.89	10	0°	10	-	-	-	-	-	10	1	6	6	7.74
L7	Topple	0.83	10	10°	10	-	-	-	-	-	10	1	6	6	7.74
L8	Wedge	1.25	6	-	-	-	-	-	-	-	6	1	8	8	6.92
L9	Topple	1.00	10	10°	10	-	-	-	-	-	10	1	8	8	8.94
L9	Topple	1.39	4	20°	10	-	-	-	-	-	4	1	6	6	4.89
L10	Wedge	0.95	10	-	-	-	-	-	-	-	10	1	6	6	7.74
L11	Wedge	1.86	2	-	-	-	-	-	-	-	2	1	6	6	3.46
L12	Wedge	1.19	7	-	-	-	-	-	-	-	7	1	6	6	6.48

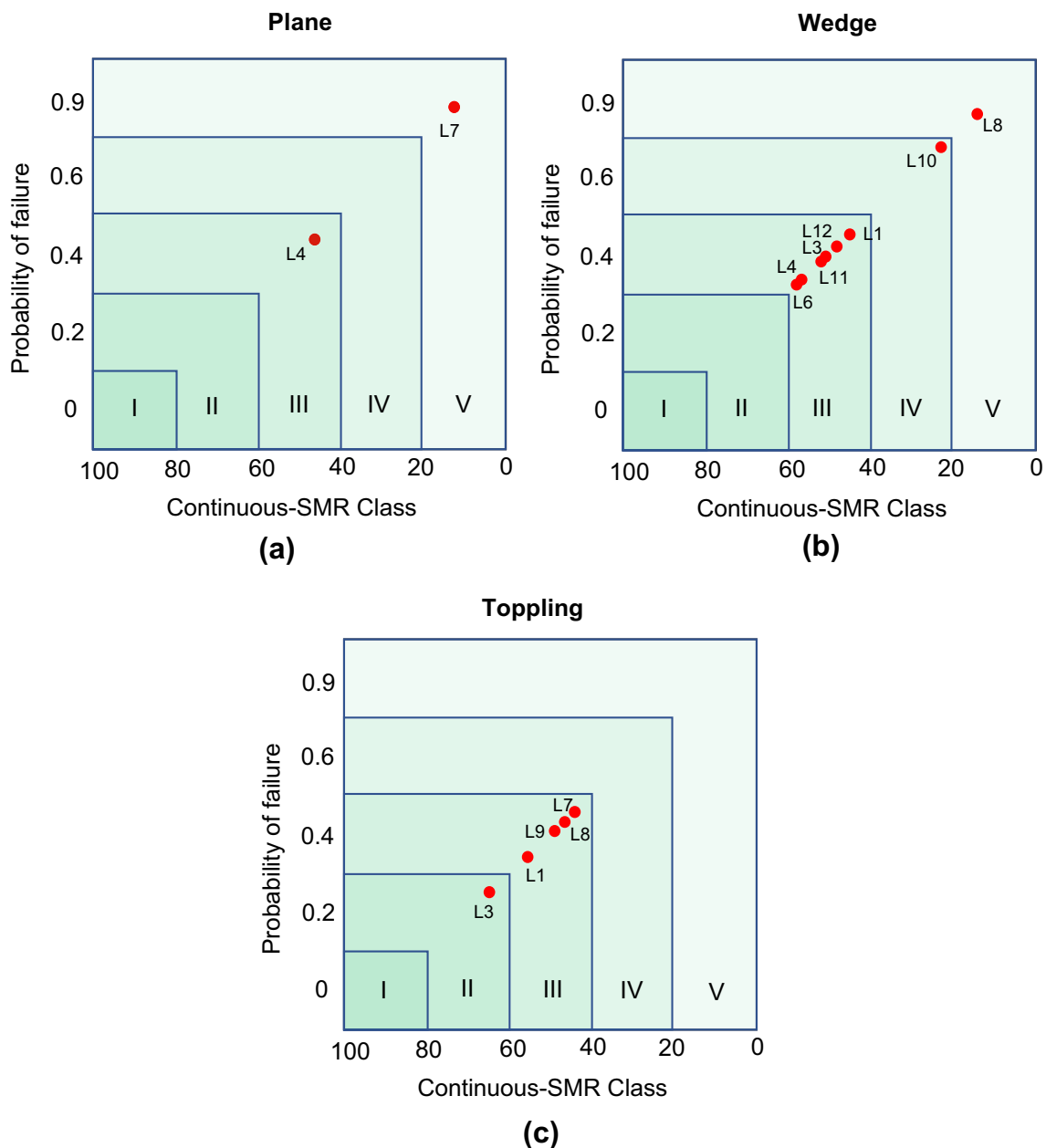


Fig. 13 The plot of Continuous SMR values and classes against their corresponding probability of failure (Romana 1985; Romana et al. 2015), for the locations of the study area for **a** Plane failure, **b** wedge failure and **c** toppling failure

with continuous SMR (scores from Table 10 and corresponding stability from Table 8), but appear unstable when classified with Q-slope (Fig. 12). The same slope has a good category HI (Table 14) for wedge and a poor category for toppling (Table 14). It is therefore proposed to combine more than one classification systems simultaneously to define empirical stability fields in the form of charts that characterizes the stability of a slope under consideration. Two of the three geomechanical classification systems – Continuous SMR, HI and Q-Slope are considered at a time to develop two-dimensional chart where the

stability fields are bounded by dark bold lines (Fig. 14). Three charts are proposed namely Chart-1, Chart-2 and Chart-3. These charts now characterize the stability of a slope more objectively.

Chart-1 (Fig. 14a) is developed by combining the stability classes of the continuous SMR and the HI. The chart includes three stability fields viz. stable, severely unstable and unstable. The slopes with structurally controlled failures are plotted in the chart to illustrate that L7 (plane), L8 (wedge) and L10 (wedge) are severely unstable.

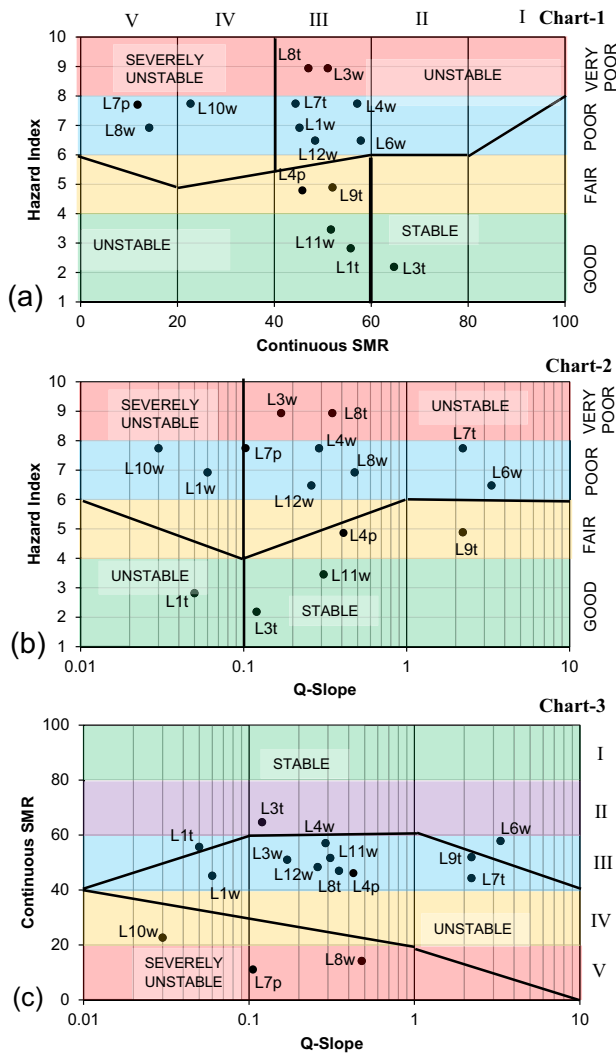


Fig. 14 Stability charts proposed in this work, based on combination of three geomechanical classification of slopes that include Continuous Slope Mass rating, Q-Slope and Hazard Index. Plots of the values of the slopes of the studied locations in the charts (p–plane, w–wedge, t–topple) are also shown. **a** Chart-1 based on Hazard index and continuous SMR, **b** Chart-2 based on Hazard Index and Q-Slope and **c** Chart-3 based on Continuous SMR and Q-Slope. In all the charts, stability fields are bound by the bold lines

Chart-2 (Fig. 14b) is developed combining the HI and the Q-Slope system and consists of three stability fields: stable, unstable and severely unstable. A plot of the scores of all slopes with structurally controlled failure in the Chart-2 reveals that L1 (wedge) and L10 (wedge) falls in the severely unstable field. It is to be noted that L1 (wedge) which is severely unstable in Chart-2 does not figure as unstable in the Continuous SMR classification whereby its score corresponds to partially stable class (Table 8) as it is having a score of 45.18 (Table 10). In Chart-2, L6 (wedge) is at the boundary between stable and unstable and therefore will be considered as unstable. L7 (plane) plots at the boundary

between severely unstable and unstable and will be considered severely unstable.

Chart-3 (Fig. 14c) is designed to combine the continuous SMR and the Q-slope systems and comprises of three stability fields: stable, severely unstable and unstable. Plots of the studied slopes in this chart shows that the slope L7 (plane), L8 (wedge) and L10 (wedge) figure as severely unstable. However, L1 (topple) and L6 (wedge) plot as stable slopes in Chart-3 but these same slopes plot as unstable in Charts-1 and 2.

In general, it is therefore suggested that all three charts be used simultaneously for slope stability assessment at a particular location and judgment has to be made accordingly. For example, if a slope is classified to be stable in one chart but unstable in other two charts, then the slope shall be treated unstable. Based on the newly proposed charts, the stability conditions of the studied slopes and the resulting judgements are summarized in Table 15.

5.3 Validation of the Proposed Charts

Assessment of the stability conditions of the slopes in the study area, based on the charts presented in Sect. 5.2 agrees well with real life slope conditions in the field and therefore stands validated. *Severely unstable* condition represents those slopes that have already failed partially and can fail further under the existing conditions, or those that are at the verge of failure or are presently failing. Slopes at locations L7, L8, and L10 belong to the severely unstable category. L7 slope is heavily jointed and have already failed by plane sliding with the plane of failure exposed (Fig. 7a). In this location, similar plane failure is imminent on blocks that await to be transported down by plane sliding (Fig. 7a). Some blocks apparently are on the verge of toppling and few already toppled down as evidenced by blocky boulders lying at the foot of the slope (Fig. 7a). Slope at location L8 is severely unstable and a part of it has wedge failed during this study (Fig. 6a). Similar wedge failure in other parts of the slope can get activated any moment under the present condition and are therefore at the verge of failure. Slope at L10 is severely unstable as it frequently shows wedge failure at several parts of the slope (Fig. 6b) where wedge blocks after failure pile up at the foot of the slope (Fig. 6b). In addition to that, slope at L10 undergoes spalling of partly weathered shells of the slope outward (Fig. 6b) that contribute to frequent rock falls.

Unstable condition represents those slopes that have potential failure surfaces or wedge axis exposed for sliding of overlying blocks or exposed tilted blocks ready for topple. From the stability charts, slopes at several locations reflect unstable conditions viz. L1, L3, L4, L6, L9, L11, and L12. Slopes of these locations in the field are in good agreement with the assessed stability conditions. For example, L4

Table 15 Stability conditions of slopes in the studied locations, based on newly proposed stability charts

Slope location	Failure type	Stability condition			Judgment and requirements
		Chart-1	Chart-2	Chart-3	
L1	Wedge	Unstable	Severely unstable	Unstable	Unstable
	Topple	Unstable	Unstable	Stable	Unstable
L2	Non- Structurally controlled failure				Unstable (From HI)
L3	Wedge	Unstable	Unstable	Unstable	Unstable
	Topple	Stable	Stable	Stable	Stable
L4	Plane	Unstable	Stable	Unstable	Unstable
	Wedge	Unstable	Unstable	Unstable	Unstable
L5	Non- structurally controlled failure				Severely unstable (From HI) especially during monsoon
L6	Wedge	Unstable	Unstable	Stable	Unstable
L7	Plane	Severely Unstable	Unstable to severely unstable	Severely unstable	Severely unstable (Requires immediate mitigation)
	Topple	Unstable	Unstable	Unstable	Unstable
	Wedge	Severely unstable	Unstable	Severely unstable	Severely Unstable (Requires immediate mitigation)
L8	Topple	Unstable	Stable	Unstable	Unstable
	Topple	Unstable	Stable	Unstable	Unstable
L9	Topple	Unstable	Stable	Unstable	Unstable
L10	Wedge	Severely Unstable	Severely Unstable	Severely Unstable	Severely Unstable (Requires immediate mitigation)
L11	Wedge	Unstable	Stable	Unstable	Unstable
L12	Wedge	Unstable	Unstable	Unstable	Unstable

is having both plane and wedge instability (Table 15) and Fig. 7b illustrates the slope condition of L4 where plane and wedge elements (indicated by black and white arrows respectively) lie exposed, along which failures have occurred earlier. Several blocks that overlie the plane and wedge elements await sliding down. The whole slope is therefore unstable.

A second example of unstable slope is L9 where instability is indicated by toppling failure. Figure 7d illustrate this condition at L9 where several blocks project out of the slope, especially at the high grounds that are likely to topple. As a validation of such unstable condition, it can be observed that some blocks have already toppled (top right corner of Fig. 7d) creating a vacant space where the toppled block originally existed.

Similarly, a third example of unstable slope condition is that of L11 where a wedge instability is indicated. This is illustrated in Fig. 7c. The large wedge block tends to slide out of the slope face along the direction of the black arrow (wedge axis). Several vacant spaces exist along the slope where wedge blocks were originally secured, have now slid down. Similar validations apply in all other locations where unstable slopes are indicated.

5.4 Comparison Between Geo-Mechanical Classification Methods for Slopes

The results of the analysis for the locations in the study area markedly vary in their scores for different parameters of evaluation (Tables 10, 11, 14). All SMR methods used in this study apply to structurally controlled failure of slopes whereas the HI is used for both structurally and non-structurally controlled slope failures. The original SMR values for every location in general are reduced to some extent while evaluating by continuous-SMR method, but in both cases the stability class and category remain unchanged. The Chinese SMR predicts a relatively higher value for each location when compared to original SMR and continuous SMR. This is due to modification of original SMR by addition of two factors i.e., the height factor ζ for slopes higher than 80 m and the discontinuity condition factor λ . For our study, since all the heights of slopes of the road-cuts are less than 80 m, the height factor ζ is taken as 1. The discontinuity factor λ induces an increase while calculating Chinese SMR. It can be observed that Chinese SMR also predicts relatively safer slope conditions that are otherwise classified as unstable or partially stable by original and continuous SMR. Therefore, the continuous-SMR is a preferred method of slope assessment since it predicts the lowest scores.

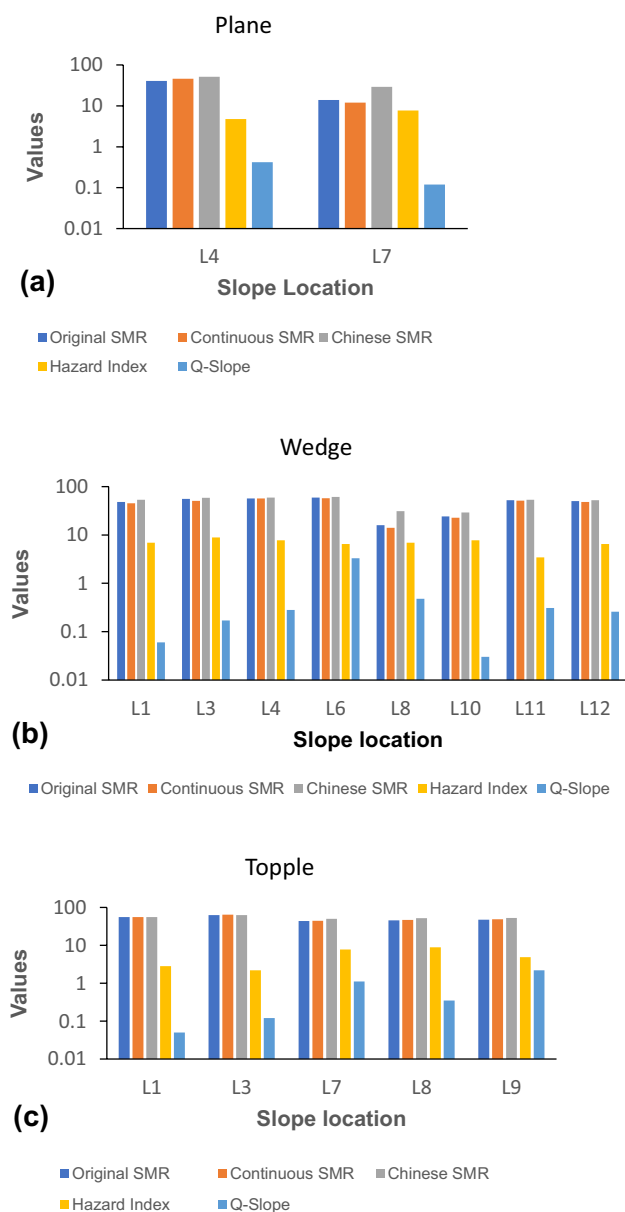


Fig. 15 Comparative column plots of original SMR, Continuous SMR, Chinese SMR, Hazard Index and Q-Slope for locations that have potential for **a** plane failure, **b** wedge failure and **c** toppling failure

The Q-Slope is important in depicting the stability status of the slope that is largely controlled by existing slope dip and its corresponding Q-slope score. The Q-slope also provides a safe slope angle amount with 1% probability of failure for unstable slopes. In addition to that the Q-slope considers the environmental conditions to which the slope is exposed and that includes rainfall and extremes of temperature which the study area is frequently exposed to. Therefore Q-Slope is a preferred method for slope stability assessment.

The HI is an important rating parameter applied for both structurally and non-structurally controlled slopes. This parameter has an added advantage of considering the effect of rainfall, surface and groundwater, vegetation and weatherability of the slope that constitute the triggering factor and are combined with subfactors for normally drained conditions of rock slopes to give a stability index. HI can therefore be clearly considered as a preferred method of slope stability assessment.

Figure 15 illustrates the column plots of all the Geomechanical classification systems of the slopes applied in the present study for the slopes that have indications of plane failure (Fig. 15a), wedge failure (Fig. 15b) and toppling failure (Fig. 15c). It can be inferred from Fig. 15a, b, that the Q-Slope is more sensitive as it distinguishes the stability of slopes with relatively more contrast when compared to continuous SMR and HI for plane and wedge failures respectively. In case of toppling failures (Fig. 15c), the HI and Q-slope are apparently both sensitive when compared with the Continuous SMR for the slopes of the study area.

5.5 Microstructural Implications on Slope Failure

Microstructural study reveals that there are several important parameters by which rock microstructure can trigger rock slope instability in the studied slope locations. The first is the anisotropy induced by foliation planes in quartzite, schistose quartzite and phyllite. Strength anisotropies of foliated rocks can be pronounced with compressive strengths varying as a function of angle (β), measured between foliation (S1) and vertically oriented compression axis (Fig. 16a) It is now well recognized that foliated rock samples loaded in orientations that result in large shear stresses resolved on the foliation plane are often several times weaker than those shortened parallel to or perpendicular to the foliation (Shea and Kronenberg 1993) as established from the experimental study of strength anisotropy of foliated rocks in compression tests (Donath 1964, McLamore and Gray 1967, Hoek 1968, Attewell and Sandford 1974, Brown et al. 1977, on shales and slates, Ramamurthy et al. 1988, on phyllites, Akai et al. 1970, McCabe and Koerner 1975, Shea and Kronenberg 1993, Behrestagi et al. 1996, Nasserri et al. 1997, 2003, Singh et al. 2001, Zhang et al. 2011 and Ferreidoooni et al. 2016 on gneisses, phyllites and schists). For tested foliated rocks, it has been established that the maximum value of cohesion and friction angles were obtained at $\beta = 90^\circ$ and $\beta = 0^\circ$, and the minimum value of these parameters were obtained at $0^\circ < \beta < 30^\circ$ and $30^\circ < \beta < 90^\circ$ respectively (Ferreidoooni et al. 2016). Hence, strength of foliated rocks is higher for values of $\beta = 0^\circ$ and $\beta = 90^\circ$, and the unconfined strength has a minimum range of 2.5–7 MPa for phyllites when $15^\circ \leq \beta \leq 30^\circ$ (Ferreidoooni et al. 2016). In the locations of

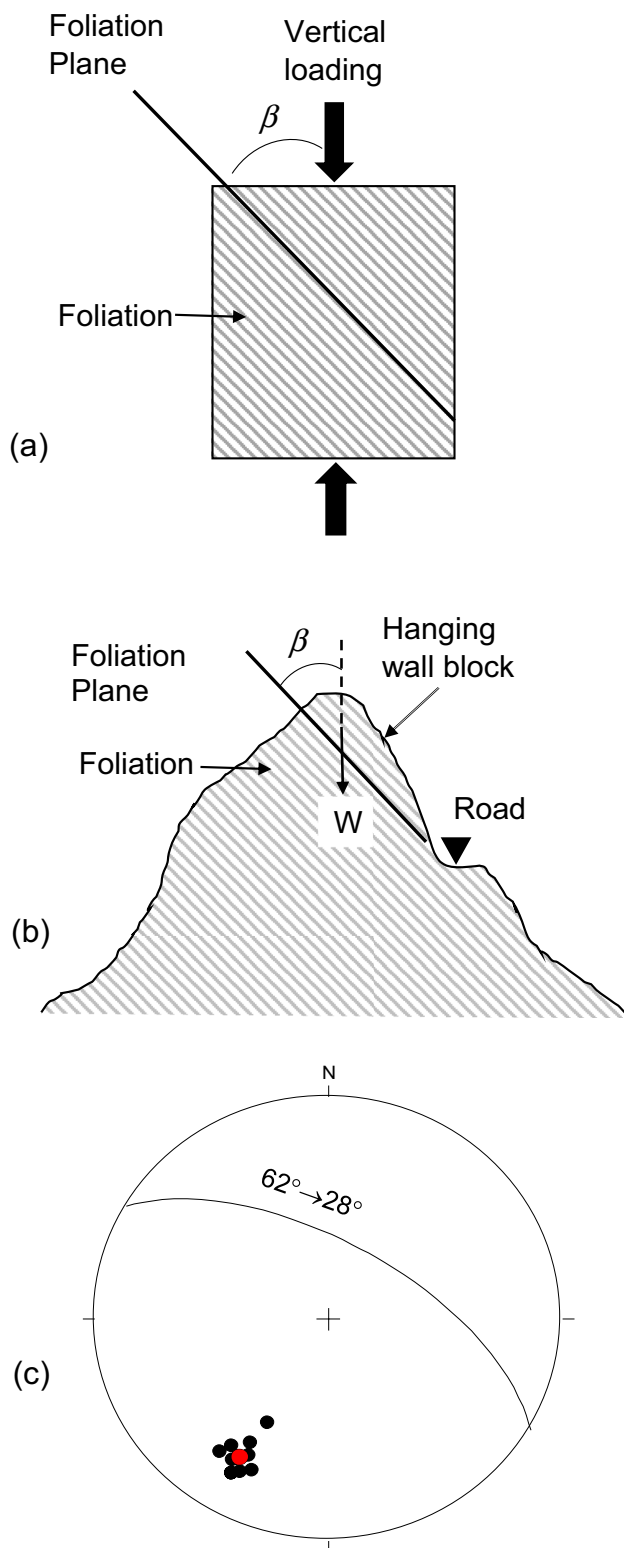


Fig. 16 Vertical loading on foliations; **a** Definition of β as angle between foliation and vertical **b** vertical loading on the foliation plane by the weight W of the hanging wall block; **c** equal area lower hemispherical projection of poles (black filled circles) to the penetrative foliation at the locations of the study area. Great circle represents the mean orientation of the foliation. Pole to mean orientation of the foliation is indicated as red filled circle

the study area, β is equivalent to the vertical component of the load of the hanging wall of the foliated rocks on the foliation plane (Fig. 16b) and the foliations have mean orientation of $62^\circ \rightarrow 28^\circ$ (Fig. 16c). The dip of the foliation (α) range $45^\circ\text{--}70^\circ$ and therefore $\beta = (90^\circ - \alpha)$ ranges $45^\circ\text{--}20^\circ$ and thus corresponds to the loading orientations ($15^\circ \leq \beta \leq 30^\circ$) of rocks that lead to reduction in cohesion, friction angle and strength along foliation joints under the influence of vertical load. The mean strength (UCS) of the phyllites with $\beta = 90^\circ$ is 30.27 MPa (Table 3) under dry condition as determined in the laboratory. This is even less than the strength of phyllites (UCS 48 MPa) when compressed with $\beta = 90^\circ$ in the experiments by Ferreidoooni et al. (2016). In the study area, the vertical stress acting on the foliation plane in phyllites located at a depth of as low as 130 m is 3.48 MPa considering the density of phyllites determined as 2.727 (Table 3). Under these conditions the phyllites are liable to fail along foliation plane if β is 20° (i.e., dip of the foliation is 70°), if the cut slope exposes the phyllites on the slope face along the dip-direction of the foliation. However, it is to be noted that the height difference between the road level on the slope and the nearest peak of the topography is frequently > 300 m and therefore the hanging wall thickness measured along vertical, above the foliation is commonly 300–400 m and is far greater than 130 m considered above. Consequently, this implies 8–10 MPa vertical stress on the foliation and that could lead to failure along foliation planes with dip amounts in the range of $56^\circ\text{--}60^\circ$, if unconfined (Fig. 2 of Ferreidoooni et al. 2016).

A second microstructural parameter that contributes to strength anisotropy is the volume percentage of mica in the foliated rocks. Several theoretical studies have shown that the strength of polyphase aggregates including quartz, feldspar, and mica depend strongly on the volume proportion of the weakest phase i.e., mica. In general, under vertical loads with $30^\circ < \beta < 90^\circ$, decreasing strength, decreasing anisotropy and increasing ductility are observed with increasing mica content in foliated rocks with volumetric proportion of mica range of 15–75% and stress–strain response and grain scale deformation microstructures in such rocks both indicate that mechanical behavior is strongly influenced by concentration and spatial arrangement of micas (Shea and Kronenberg 1993). In the study area mica volume proportions vary between 15% (quartzite) to 80% (phyllite) and micas define the cleavage by strong shape preferred orientation in schist and phyllite (Fig. 10b, c). This therefore indicate the possibility of slip by ductile glide along mica long dimensions in the mica-rich cleavage domains under persistent vertical load on dipping foliations emulating the condition $30^\circ < \beta < 90^\circ$. Possibility of failure based on the above microstructural properties apply to the slopes of L8.

The third and a very important parameter is the presence of water seepage pathways along foliation planes that can largely reduce friction angle along discontinuities and cleavage planes due to lubrication effect or water-induced decomposition of rock material along foliation, if water infiltrates during heavy rainfall. For example, in location L9 (Fig. 9, L9), only toppling failure is indicated by kinematic analysis. The wedge axis formed by intersection of joints J2 and J3 lies outside the friction circle and therefore a wedge failure is precluded. However, if infiltrated water along foliation planes and J2 and J3 act as a lubricant and increase the water pressure and thereby decrease the friction angle of the discontinuities, then the diameter of the friction circle may become large enough in the stereogram of L9 in Fig. 9 to contain the wedge axis inside it. Consequently, a wedge failure then becomes kinematically possible, in addition to the toppling failure in L9 (Fig. 9). In such a situation the foliations will act as a release surface since they dip towards northeast. This is true for all those locations where such conditions apply.

5.6 Integrating Rock Microstructure with Proposed Stability Charts

As indicated in Fig. 3, the final judgment on slope stability condition should be formed after integration of microstructural information with the geomechanical stability information from the proposed charts. The importance of this integration stems out from the fact that geomechanical stability condition of slopes may be additionally influenced by rock microstructure and composition as discussed in the previous section. Weakening of cohesive strength along penetrative foliation planes due to water seepage may induce a failure along foliation plane in an otherwise 'stable' looking slope especially during monsoons.

Some slopes that have been identified as unstable from the proposed stability charts may convert to 'severely unstable' category if the slope contain appropriately oriented 'day-lighted' foliation planes that are dominantly defined by mica and where volume percentage of mica is relatively higher in the foliated rocks that dip out from the slope. This is often the case when phyllites and slates are intercalated with other rock types that constitute a slope, for example L1, L8, L9 and L10.

In the study area, foliations are sometimes parallel or sub-parallel to one set of joint (for example J3 in L8) and sometimes at an angle to other joint set (for example J2 in L8). This forms a favorable situation for water to permeate through J2 and soak and seep through the foliations and consequently increases the tendency of the foliated block of rock overlying J3 to slide along J3. L8 has already been identified as a severely unstable slope. Likewise, other unstable slopes need to be further examined for their 'severity', if any, caused by rock microstructure and composition.

5.7 Interlink and Interdependence Between the Studied Parameters

The parameters used in this study, indicate particular conditions of slopes when studied individually, and also provides new information on the stability conditions of rock slopes when interlinked and studied in combinations. Natural slope distribution controls the steepness of slopes at different locations along the highway. Where valleys dissect spurs and intersect the road section, the slopes are relatively gentler compared to those on spurs and do not pose any risk of slope failures. However, these points may be hazardous during the monsoons at peak precipitation times due to surface run-off. The orientation of the cut-slope face depends on the natural slope distribution and the method of excavation and are therefore interlinked. The kinematic analysis involving orientations of cut slope and discontinuities and internal friction angle are therefore linked to the distribution and orientation of natural slopes. The several slope mass rating parameters used in this study generated rating scores using engineering properties of rocks, slope height, slope vegetation, rainfall, weatherability, rock mass properties, type of kinematic failure possibilities and geometric orientation of – natural slopes, slope face and discontinuities in various combinations and thereby indicate the interdependence of the parameters. Microstructural characterization provides additional information on directional anisotropy and evidence of water circulation along incipient planes parallel to rock cleavage and both of which can contribute to slope failure by strength reduction during the monsoon along planes that are apparently safe in dry conditions. Microstructures contributing to directional anisotropy also controls the engineering geological properties of rocks viz. UCS, PLSI and tensile strength and are therefore interlinked.

6 Conclusions

A multi-parametric integrated approach has been adopted in the study of slope stability assessment along a stretch of Dharasu-Uttarkashi highway in the topographically rugged terrains of the Lesser Himalayas in India. The parameters used in the study include distribution of steepness of natural slopes, field observations and new data on existing slope failures, cut-slope height, cut-slope face orientation, number of discontinuities and their orientations, structural elements, rock mass characteristics, weatherability, kinematic analysis of slopes, rock microstructures and geomechanical classification of slopes. The parameters are all interlinked and interdependent and therefore yield results and information on stability conditions of road-cut slopes that are fairly comprehensive. Based on the combined study of the above parameters, the assessment of stability of road-cut slopes in the study area has been performed for twelve locations (L1–L12) on the road-cut sections where

the slopes have not yet failed. A new set of stability charts is developed on the basis of continuous slope mass rating, hazard index and Q-Slope systems of geomechanical classification of slopes. The slopes with possibility of structurally controlled failure were classified on the basis of this newly proposed stability charts as one of the three types: severely unstable, unstable and stable. The slopes whose failure potentials are not structurally controlled were assessed to have a Hazard Index of poor to very poor category and could lead to rainfall-induced failures. Based on new stability charts, slopes at locations L7, L8 and L10 were assessed to be severely unstable. Rock microstructural strength anisotropy and water seepage along foliation planes can additionally induce failure in slope locations L1, L8, L9 and L10, especially during monsoons. From reconnaissance, it was observed that, particularly in the southern side beyond the study area, several other sections of the Dharasu-Uttarkashi roadway are threatened by slope instabilities. Similar studies in those sections need to be performed systematically in future to ensure safety of the entire roadway.

Acknowledgements AKG is grateful to IIT(ISM) Dhanbad for providing fellowship and necessary support for carrying out the work. MKM gratefully acknowledges financial support from the Science and Engineering research Board, Department of Science and Technology (Govt. of India) for this research under Project No. SR/S4/ES-516/2010 and financial assistance from PDA fund of IIT(ISM) Dhanbad for undertaking fieldwork, data analysis and laboratory testing of rock samples. The authors would also like to thank Prof. A. K. Mishra of Department of Mining Engineering IIT (ISM) Dhanbad for providing instrumental facility and Mr. B. Munshi for technical support during experimental work.

Author contributions AKG— Fieldwork, data and sample collection, sample preparation, laboratory testing, data analysis and drafting of some of the figures. MKM— Fieldwork, data and sample collection, laboratory testing, methodology development, generation of data on Rock mass characterization, geomechanical classification of slopes and rock microstructure, Research on data, complete manuscript writing.

Funding A K Gupta acknowledges the Ministry of Human Resource Development (MHRD) funded fellowship and support provided by the Indian Institute of Technology (ISM) Dhanbad, India. M. K. Mukherjee has been funded by the PDA awarded to him by IIT(ISM) Dhanbad and partly from financial support from the Science and Engineering Research Board, Department of Science and Technology (Govt. of India) for this research under Project No. SR/S4/ES-516/2010 awarded to him.

Declarations

Conflict of Interest The authors hereby declare that there is no conflict of interest in the present work.

References

Akai K, Yamamoto K, Arioka M (1970) Experimental research on the structural anisotropy of crystalline schists. *Proc Int Congress Rock Mech* 2:181–186

- Aksoy C (2008) Review of rock mass rating classification: historical developments, applications, and restrictions. *J Min Sci* 44:51–63
- Anbalagan R, Sharma S, Raghuvanshi TK (1992) Rock mass stability evaluation using modified SMR approach. In: Jha, P.C. (ed.), *Rock Mechanics: Proceedings of the Sixth National Symposium on Rock Mechanics*. Springer, Berlin, pp 258–268
- Attewell PB, Sandford MR (1974) Intrinsic shear strength of a brittle anisotropic rock—I; experimental and mechanical interpretation. *Int J Rock Mech Min Sci* 11:423–430
- Bar N, Barton N (2017) The Q-slope method for rock slope engineering. *Rock Mech Rock Eng* 50:3307–3322
- Barton N, Grimstad E (2014) Forty years with the Q-system in Norway and abroad. *Fjellsprengningsteknikk, Bergmekanikk/geoteknikk, NFF, Oslo* 4(1–4):25
- Barton N, Lien R, Lunde J (1974) Engineering classification of rock masses for the design of tunnel support. *Rock Mech* 6:189–223
- Barton N, Bar N (2015) Introduction to Q-slope method and its intended use within civil and mining engineering projects. In: *ISRM European Regional Symposium-EUROCK 2015, Salzburg, Austria, International Society for Rock Mechanics and Rock Engineering*, Oct. 7–10, pp 157–162
- Basahel H, Mitri H (2017) Application of rock mass classification systems to rock slope stability assessment: a case study. *J Rock Mech Geotech Eng* 9:993–1009
- Behrestaghi MHN, Rao KS, Ramamurthy T (1996) Engineering geological and geotechnical responses of schistose rocks from dam project areas in India. *Eng Geol* 44:183–201
- Bieniawski ZT (1973) Engineering classification of jointed rock masses. *Civil Engr S Afr* 15:335–343
- Bieniawski ZT (1989) *Engineering rock mass classification*. Wiley, Chichester, p 251
- Brown ET, Richard LR, Barr MV (1977) Shear strength characteristics of Delabole slates. In: *Proceedings of conference for rock engineering*. Tyne, Newcastle, pp 31–51
- Chen Z (1995) Recent developments in slope stability analysis. In: Fuji T (ed) *Keynote lecture: proceedings of 8th international congress on rock mechanics*, 3rd edn. Springer, Berlin, pp 1041–1048
- Chen Q, Yin T (2020) Modification of the rock mass rating system (RMR_{mbi}) considering three-dimensional rock block size. *Bull Eng Geol Environ* 79:789–810
- Deere DU (1963) Technical description of rock cores for engineering purposes. *Felsmechanik Und Ingenieurgeologie (rock Mech Eng Geol)* 1:16–22
- Deere DU, Hendron AJ, Patton F, Cording EJ (1967) Design of surface and near surface excavations in rock. In: Fairhurst C (ed) *Proceedings of the 8th US symposium on rock mechanics: failure and breakage of rock*. AIME, New York, pp 237–302
- Donath FA (1964) Strength variation and deformational behavior of anisotropic rocks. *State of stress in the Earth's crust*. Elsevier, New York
- Fereidooni D, Khanlari GR, Heidari M, Sepahigero AA, Kolahi-Azar AP (2016) Assessment of inherent anisotropy and confining pressure influences on mechanical behavior of anisotropic foliated rocks under triaxial compression. *Rock Mech Rock Eng* 49:2155–2163
- Goodman RE (1989) *Introduction to rock mechanics*, 2nd edn. Wiley, New York, p 562
- Gray DR (1978) Cleavages in deformed psammitic rocks from southeastern Australia: their nature and origin. *Geol Soc Am Bull* 89:577–590
- Gupta V, Tandon RS (2015) Kinematic rockfall hazard assessment along a transportation corridor in the upper Alakanada valley, Garhwal Himalaya, India. *Bull Eng Geol Environ* 74:315–326
- Hack HR (1998) *Slope stability probability classification*. ITC Delft Publications ITC, Enschede, p 275

- Hack R, Price D, Rengers NA (2003) A new approach to rock slope stability—a probability classification (SSPC). *Bull Eng Geol Environ* 62:167–184
- Haines A, Terbrugge PJ (1991) Preliminary estimation of rock slope stability using rock mass classification system. In: Wittke W (ed) *Proceedings of the 7th international congress on rock mechanics*. Balkema, Rotterdam, pp 887–892
- Harrison JP, Hudson JA (2000) *Engineering rock mechanics: Illustrative worked examples*. Elsevier Science, Oxford, p 530
- Hoek E (1968) Brittle failure of rock. *Rock mechanics in engineering practice*. Wiley, London
- Hoek E (1983) Strength of jointed rock masses, 1983 Rankine Lecture. *Geotechnique* 33(3):187–223
- Hoek E (1994) Strength of rock and rock masses. *ISRM News J* 2(2):4–16
- Hoek E, Bray JW (1981) *Rock slope engineering*, 3rd edn. Institute of Mining and Metallurgy, London, p 358
- Hoek E, Brown ET (1980) *Underground excavations in rock*. The Institution of Mining Metallurgy, London, p 527
- Hoek E, Brown ET (1988) The Hoek-Brown failure criterion - a 1988 update. In: *Proceedings of the Fifteenth Canadian Rock Mechanics Symposium*, University of Toronto, pp 31–38.
- Hoek E, Brown ET (1997) Practical estimates of rock mass strength. *Int J Rock Mech Min Sci* 34(8):1165–2118
- Hoek E, Wood D, and Shah S (1992) A modified Hoek-Brown criterion for jointed rock masses. In: *Proceedings of the ISRM Symposium: Eurock'92*, Thomas Telford, pp 209–221
- Hoek E, Kaiser PK, and Bawden WF (1995) *Support of Underground Excavations in Hard Rock*. A.A. Balkema, Rotterdam, 214 pp.
- Hoek E, Marinos P, Benissi M (1998) Applicability of the geological strength index (GSI) classification for very weak and sheared rock masses: the case of the Athens schist formation. *Bull Eng Geol Environ* 57:151–160
- ISRM (1981) The ISRM suggested methods for determining the uniaxial compressive strength and deformability of rock materials. In: Brown ET (ed) *Rock Characterization, Testing and Monitoring—ISRM Suggested Methods*. Pergamon, London, pp 111–116
- Jain AK, Dasgupta S, Bhargava ON, Israil M, Perumal RJ, Patel RC, Mukul M, Parcha SK, Adlakha V, Agarwal KK, Singh P, Bhat-tacharyya K, Pant NC, Banerjee DM (2016) Tectonics and evolution of the Himalaya. *Proc Indian Natl Sci Acad* 82:581–604
- Kentli B, Topal T (2004) Assessment of rock slope stability for a segment of the Ankara-Pozanti motorway, Turkey. *Eng Geol* 74:73–90
- Kumar P, Kumar A, Sinval A (2011) Assessment of seismic hazard in Uttarkhand Himalaya. *Dis Prev Manag* 20:531–542
- Laubscher DH (1990) A geomechanical classification system for the rating of rock mass in mine design. *J s Afr Instit Min Metallurgy* 90:257–273
- Lindsay P, Campbell RN, Fergusson DA, Gillard GR, Moore TA (2001) Slope stability probability classification, Waikato Coal Measures, New Zealand. *Int J Coal Geol* 45:127–145
- Liu Y, Chen C (2007) A new approach for application of rock mass classification on rock slope stability assessment. *Eng Geol* 89:129–143
- Marinos P, Hoek E (2001) Estimating the geotechnical properties of heterogeneous rock masses such as flysch. *Bull Eng Geol Environ* 60:85–92
- Marinos V, Marinos P, Hoek E (2005) The Geological Strength Index: applications and limitations. *Bull Eng Geol Environ* 64:55–65
- Marinos P, Hoek E (2000) GSI: A geologically friendly tool for rock mass strength estimation. In: *Proceedings of the International Conference on geotechnical and geological engineering (Geo-Eng2000)*, Melbourne, Nov. 19–24, pp 1422–1442
- McCabe WM, Koerner RM (1975) High pressure shear strength investigation of an anisotropic mica schist rock. *Int J Rock Mech Min Sci Geomech Abstr* 12:219–228
- McLamore R, Gray KE (1967) The mechanical behavior of anisotropic sedimentary rocks. *Trans Am Soc Mech Eng B* 89:62–76
- Nasseri MHB, Rao KS, Ramamurthy T (1997) Failure mechanism in schistose rocks. *Int J Rock Mech Min Sci* 34:3–4
- Nasseri MHB, Rao KS, Ramamurthy T (2003) Anisotropic strength and deformational behavior of Himalayan schists. *Int J Rock Mech Min Sci* 40:3–23
- Pantelidis L (2009) Rock slope stability assessment through rock mass classification systems. *Int J Rock Mech Min Sci* 46:315–325
- Pantelidis L (2010) An alternative rock mass classification system for rock slopes. *Bull Eng Geol Environ* 69:29–39
- Powell MA (1979) A morphological classification of rock cleavage. *Tectonophysics* 58:21–34
- Pradhan SP, Siddique T (2020) Stability assessment of landslide-prone road cut rock slopes in Himalayan terrain: a finite element method based approach. *Journal of Rock Mechanics and Geotechnical Engineering* 12(1):59–73
- Ramamurthy T, Rao GV, Singh J (1988) A strength criterion for anisotropic rocks. In: *Proceedings of International symposium on rock at great depth*. Pau, France, pp 37–44
- Robertson AM (1988) Estimating weak rock strength. In: Sastry, K.V.S. (Ed.), *Proceedings of the SME Annual Meeting*. Society of Mining Engineering, Phoenix, Arizona, Jan. 25–28, pp 1–5
- Rocscience Inc. (2014) *DIPS v. 6.0 graphical and statistical analysis of orientation data*. Toronto, Canada.
- Romana M (1985) New adjustment ratings for application of Bieniawski classification to slopes. In: *Proceedings of International Symposium on the Role of Rock Mechanics in Excavations for Mining and Civil Works*, ISRM, Zacatecas, Sep. 2–4, pp 49–53
- Romana M (1993) A geomechanical classification for slopes: slope mass rating. In: Hudson JA (ed) *Comprehensive rock engineering*. Pergamon Press, Oxford, pp 575–599
- Romana M, Tomás R, Serón JB (2015) Slope Mass Rating (SMR) Geomechanics classification: thirty years review. In: *ISRM Congress 2015 Proceedings - International Symposium on Rock Mechanics*, Quebec, Canada, May 10–13 2015. ISBN: 978-1-926872-25-4, pp 10
- Selby MJ (1980) A rock mass strength classification for geomorphic purposes, with test from Antarctica and New Zealand. *Z Für Geomorphologie* 24:31–51
- Sen Z, Sadagah BH (2003) Modified rock mass classification system by continuous rating. *Eng Geol* 67:269–280
- Shanker R, Kumar G, Saxena SP (1989) Stratigraphy and sedimentation in Himalaya; a reappraisal. *Geol Tecton Himal Geol Surv India Spl Pub* 26:1–60
- Sharma R, Singh PN (2005) *Compiled Map of Dehradun Quadrangle 53J, Uttaranchal, India*; Geological Survey of India, Northern Region, Lucknow
- Shea WT, Kronenberg AK (1993) Strength and anisotropy of foliated rocks with varied mica contents. *J Struc Geol* 15:1097–1121
- Shuk T (1994) Key elements and applications of the natural slope methodology (NSM) with some emphasis on slope stability aspects. In: *Proceedings of the 4th South American Congress on Rock Mechanics*, Santiago, May 10–14 pp 255–266
- Singh VK, Singh D, Singh TN (2001) Prediction of strength properties of some schistose rocks from petrographic properties using artificial neural networks. *Int J Rock Mech Min Sci* 38:269–284
- Sönmez H, Ulusay R (1999) Modifications to the geological strength index (GSI) and their applicability to stability of slopes. *Int J Rock Mech Min Sci* 36:743–760
- Sönmez H, Ulusay R (2002) Discussion on the Hoek-Brown failure criterion and suggested modifications to the criterion verified by slope stability case studies. *Yerbilimleri* 26:77–99

- Strahler A (1957) Quantitative analysis of watershed geomorphology. *Trans Am Geophys Union* 38:913–920
- Taheri A, Tani K (2010) Assessment of the stability of rock slopes by the slope stability rating classification system. *Rock Mech Rock Eng* 43:321–333
- Tomás R, Delgado J, Serón JB (2007) Modification of slope mass rating (SMR) by continuous functions. *Int J Rock Mech Min Sci* 44:1062–1069
- Tomás R, Cuenca A, Cano M, García-Barba J (2012) A graphical approach for slope mass rating (SMR). *Eng Geol* 124:67–76
- Turner AK, Schuster RL (1996) Landslides—investigation and mitigation. Transportation Research Board, National Research Council, Special Report, 247th edn. National Academy Press, Washington, p 673
- Umrao RK, Singh R, Ahmad M, Singh TN (2011) Stability analysis of cut slopes using continuous slope mass rating and kinematic analysis in Rudraprayag District, Uttarkhand. *Geomaterials* 1:79–87
- Ünal E (1996) Modified rock mass classification: M-RMR system. In: Bieniawski ZT (ed) *Milestones in rock engineering*. The Bieniawski Jubilee Collection, Balkema, pp 203–223
- Wyllie DC, Mah C (2004) *Rock slope engineering (civil and mining)*, 4th edn. CRC Press, London, p 431p
- Yin A (2006) Cenozoic tectonic evolution of the Himalayan orogen as constrained by along-strike variation of structural geometry, exhumation history, and foreland sedimentation. *Earth Sci Rev* 76:1–131
- Zhang XP, Wong LNY, Wang SJ, Han GY (2011) Engineering properties of quartz mica schist. *Eng Geol* 121:135–149

Publisher's Note Springer Nature remains neutral with regard to jurisdictional claims in published maps and institutional affiliations.